Step-like growth of the continental crust in South China: evidence from detrital zircons in Yangtze River sediments

Zheng-Wei Liang [a,b,*], Shan Gao [a,b], Chris J. Hawkesworth [c], Yuan-Bao Wu [a,b], Craig D. Storey [d], Lian Zhou [a], Ming Li [a], Zhao-Chu Hu [a], Yong-Sheng Liu [a,b], Xiao-Ming Liu [e]

[a] State Key Laboratory of Geological Processes and Mineral Resources, China University of Geosciences, Wuhan 430074, China
[b] School of Earth Sciences, China University of Geosciences, Wuhan 430074, China
[c] Earth Sciences Department, University of Bristol, Bristol BS8 1RJ, UK
[d] School of Earth and Environmental Sciences, University of Portsmouth, Portsmouth PO1 3QL, UK
[e] State Key Laboratory of Continental Dynamics, Department of Geology, Northwest University, Xi'an, 710069, China

ABSTRACT

Detrital zircons from nine river sand samples from the upper, middle and lower streams of the Yangtze River (the world's third largest river) and its two largest tributaries, the Han and Jialing rivers have been analyzed for U–Pb–Lu–Hf–O isotope compositions. Zircons from the upper Yangtze River cluster in age groups at 0–100, 200–300, 400–500, 700–1000, 1800–1900 and 2300–2500 Ma, with a marked peak at 41 Ma diagnostic of magmatism on the Tibetan Plateau. Zircons from the middle and lower Yangtze River and its tributaries exhibit broadly similar age groups at 100–300, 400–500, 700–900, 1800–2000 and 2300–2700 Ma, except for the lack of Cenozoic ages.

The Yangtze River catchment is covered by thick Phanerozoic sedimentary rocks and so Archean-aged zircons are likely to be under-represented in modern river sands. We therefore applied the approach of Dhuime et al. (2012) to calculate a crustal growth curve for South China, and the resultant curve has two inflections. The older inflection at ~2.8 Ga is slightly younger than that of Dhuime et al. (2012), suggesting the onset of plate tectonics in the Yangtze Craton. The younger inflection at ~1.8 Ga appears to mark the onset of another period of relatively high crustal growth rate in South China. This period of increased crustal growth rate in the Mesoproterozoic is coeval with the breakup of the supercontinent Columbia, suggesting that the Mesoproterozoic crustal growth in South China may be related to supercontinent dispersal.

Comparison with global crustal growth curves based on detrital zircons highlights the distinct step-like pattern of crustal growth in South China. This emphasizes the potential of comparing regional with global crustal growth curves, and the changes in the rates of crustal growth in South China appear to have been controlled by changes in regional geodynamics. The maximum $\delta^{18}O$ values in the zircons analyzed increase markedly at the end of the Archaean, and these increases therefore accompany the estimated increases in atmospheric oxygen at that time. It is therefore suggested the atmospheric O_2 levels were associated with increased crustal weathering, the development of more elevated $\delta^{18}O$ sediments and their increasing incorporation in the generation of crustally derived magmas from ca. 2.5 Ga.

© 2018 Published by Elsevier B.V.

1. Introduction

The continental crust is a major consequence of Earth's differentiation. Its formation influences the compositions of the mantle and the atmosphere (Hawkesworth and Kemp, 2006; Lee et al., 2016), and it has been argued, for example, that the rise in atmospheric oxygen is linked to the formation and evolution of the continental crust (Lee et al., 2016). Thus, the rates of growth of the continental crust, and how that has changed with time, remain fundamental questions in Earth sciences. Clastic sediments and sedimentary rocks provide accessible samples for studying the chemical composition and growth of the continental crust for elements that are relatively insensitive to weathering (Rudnick and Gao, 2003). Zircon, a common accessory mineral in sedimentary rocks, is resistant to high temperature and pressure alteration even after recycling into mantle depths (Claoue-Long et al., 1991; Zheng et al., 2006). Zircon can be precisely analyzed in situ for U–Pb ages and for Lu–Hf–O isotopes and trace element compositions by Secondary

Ionization Mass Spectrometry (SIMS) and Laser Ablation Inductively Coupled Plasma Mass Spectrometry (LA-(MC)ICP–MS). Integration of zircon U–Pb–Lu–Hf–O isotope compositions constrains the age and nature of the magmas from which the zircons crystallized. Detrital zircons from large rivers sample zircons in the exposed rocks of large drainage areas, and they have therefore been widely used to study the formation and evolution of the continental crust (Iizuka et al., 2010).

The Yangtze River is the world's third largest river with a total length of 6418 km and a total drainage area of 1,808,500 km^2, which accounts for almost one fifth of the land area of China. Iizuka et al. (2010) analyzed U–Pb ages and Hf isotopic compositions of detrital zircons from one sand sample collected in the lower reaches of the Yangtze River at Nanjing. He et al. (2013) determined U–Pb ages and Hf isotope ratios of detrital zircons from ten sand samples along the Yangtze River and its tributaries. However, neither of these studies reported zircon oxygen isotopic compositions, which remain critical in identifying zircons that crystallized from magmas that contain contributions from sediments, which are themselves often mixtures of material from different source terrains. Thus, the Hf model ages of zircons from magmas that include a sedimentary contribution remain difficult to interpret (Hawkesworth et al., 2010; Hawkesworth and Kemp, 2006; Kemp et al., 2006).

In this study, we report U–Pb ages and Lu–Hf–O isotope compositions of detrital zircons from nine sand samples from the upper, middle and lower streams and at the mouth of the Yangtze River, and from two of its largest tributaries, the Han and Jialing rivers (Fig. 1). These results are integrated with the results from previous studies (He et al., 2013; Iizuka et al., 2010; Li et al., 2012; Liu et al., 2008; Wang et al., 2011) and provide new insights into the formation and evolution of the crust in South China.

2. Geological background and sampling

The Yangtze River originates in the Tanggula Mountain, the eastern part of the Qinghai–Tibetan Plateau and empties into the East China Sea. It traverses a number of different tectonic units, including the Northern Qiangtang Terrane, the Songpan–Ganze Fold Belt, the Qinling–Dabie Orogenic Belt, the Yangtze Craton and the Cathaysia Block (Fig. 1). The upper reaches of the Yangtze River are divided into three parts, downstream, from west to east: the Tuotuo River, the Tongtian River and the Jinsha River (Fig. 1). Three sand samples were collected from the Tuotuo, Tongtian and Jinsha rivers, three are from

the Han and Jialing rivers, and the remaining three samples are from the Yangtze River itself. The sample information is given in Table 1.

The Qiangtang Terrane lies in the north-central Tibetan Plateau. It is divided into the Northern and Southern Qiangtang Terranes separated by a high-pressure metamorphic belt in the central part (Chen et al., 2016 and references therein). The only dated basement rocks in the whole of the Qiangtang Terrane are orthogneisses with ages of 476–471 Ma from the Duguer Mountain (Pullen et al., 2011). Paleoproterozoic crustal basement may underlie this area, although this has yet to be established geochronologically (Peng et al., 2015). The NQT is mainly covered by Triassic–Cretaceous sedimentary rocks with minor volumes of Late Plaeozoic sediments (Peng et al., 2015 and references therein). The youngest age of ~618 Ma for detrital zircons from the Ningduo Group indicate that the oldest sedimentary rocks in the NQT are Late Neoproterozoic in age (He et al., 2011). Triassic igneous rocks mainly outcrop along the southern margin of the NQT (Chen et al., 2016). The rocks with younger Hf model ages of ca. 1.0 Ga are thought to have been formed by the melting of subducted oceanic crust, whereas those with older Hf model ages of ~1.7–2.1 Ga are considered to have been derived from the Proterozoic crustal basement (Peng et al., 2015). Cenozoic volcanic rocks are widespread in the Qiangtang Terrane, ranging in age from 65 to 26 Ma (Xia et al., 2011).

The Songpan–Ganze Fold Belt (SGFB) is composed of middle to late Triassic flysch sediments with thicknesses of up to 15 km (Bruguier et al., 1997). The proximal provenances of these flysch sediments are considered to be the Qinling–Dabie Orogen (Weislogel et al., 2006) and the southern margin of the North China Craton (Bruguier et al., 1997; Weislogel et al., 2006), together with minor contributions from the Kunlun arc and the Yangtze Craton (Bruguier et al., 1997). Triassic post-collision adakites and granitoids are widely distributed in the Songpan–Ganze Fold Belt (Zhang et al., 2006a). Detrital zircons from Triassic sediments and river sands within the SGFB cluster in four age groups at 250–280, 400–450, 1850–1950 and 2400–2500 Ma (He et al., 2013; Weislogel et al., 2006; Zhang et al., 2014). The Nd model ages of these rocks range from ca. 1.3–1.6 Ga suggesting that there is unexposed Proterozoic basement in the SGFB (Zhang et al., 2006a). Detrital zircons from the Triassic flysch sediments exhibit three major age peaks at 0.2–0.5, 0.75–1.0 and 1.7–2.0 Ga, and the Hf isotopic data indicate that the Neoarchean was an important period of continental growth, and that the Phanerozoic was dominated by crustal reworking with insignificant addition of juvenile crust (Zhang et al., 2014).

The drainage area of the Yangtze River includes the South Qinling and South Dabie–Sulu Orogenic Belts, both of which are thought to
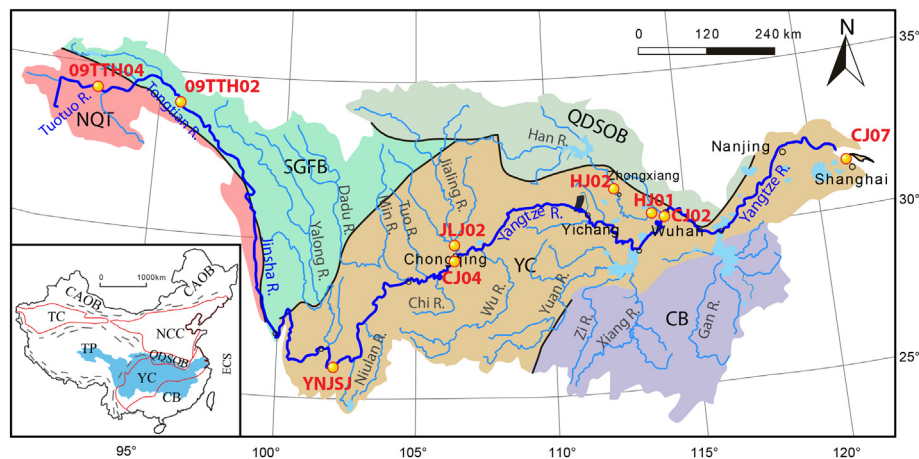
Fig. 1. A simplified geological map of the Yangtze River drainage area, modified from He et al. (2013). Thick blue curve indicates the mainstream of the Yangtze River and thin blue curves are its tributaries. Solid circles with sample numbers indicate the samples analyzed in this study. The small black area indicates exposed Archean Kongling Terrane. The letter "R." is the abbreviation of "River". The inset shows the tectonic divisions of China, where the filled blue area indicates the drainage area of the Yangtze River and its tributaries. CAOB = Central Asian Orogenic Belt; TC = Tarim Craton; NCC = North China Craton; TP = Tibetan Pleatou; NQT = Northern Qiangtang Terrane; SGFB = Songpan–Ganze Fold Belt; QDSOB = Qinling–Dabie–Sulu Orogenic Belt; YC = Yangtze Craton; CB = Cathaysia Block; ECS = East China Sea.

Table 1
Summary of sample information

Sample	Rock type	Location	Latitude (N°)	Longitude (E°)
09TTH04	Tuotuo river sand	Golmud	34°13′14.22″	92°26′39.84″
09TTH02	Tongtian river sand	Qumarleb County	34° 2′8.82″	95°49′21.90″
YNJSJ	Jinsha river sand	Lijiang	25°57′51.00″	101°52′48.00″
JLJ02	Jialing river sand	Chongqing	29°34′20.00″	106°34′58.00″
CJ04	Yangtze river sand	Chongqing	29°34′12.00″	106°35′5.00″
HJ02	Han river sand	Zhongxiang	31°11′12.42″	112°33′32.34″
HJ01	Han river sand	Wuhan	30°35′12.78″	114°12′2.10″
CJ02	Yangtze river sand	Wuhan	30°33′40.74″	114°17′43.80″
CJ07	Yangtze river sand	Shanghai	31°27′54.96″	121°24′47.70″
LT07[a]	Sandstone	Yiching	30°33′26″	111°03′21″
GCH01[a]	Tillite	Yiching	30°33′26″	111°03′21″

[a] LT07 and GCH01 are from X. M. Liu's paper that is being prepared.

belong to the northern margin of the Yangtze Craton (Chen and Jahn, 1998; Dong et al., 2011). The South Qinling Orogenic Belt consists of Meso-Neoproterozoic basement intruded by a number of Neoproterozoic plutons and large swarms of Early Paleozoic mafic and felsic rocks (Wang et al., 2017). These rocks are covered by Neoproterozoic to Triassic sedimentary sequences (Dong et al., 2011). Triassic granitoids typically outcrop in the western South Qinling Orogenic Belt (Dong et al., 2011 and references therein; Luo et al., 2012). They have whole rock Nd model ages ranging from 1.35–1.70 Ga and zircon Hf model ages of 0.94–1.5 Ga, suggesting Meso-Paleoproterozoic crustal sources (Luo et al., 2012). The Dabie–Sulu Orogenic Belt is the eastward extension of the Qinling Orogenic Belt. Mesozoic magmatism in the Dabie Orogen is post-collisional and composed of voluminous early Cretaceous granitoids with minor gabbros (Chen et al., 2002).

The Yangtze Craton underlies nearly 70% of the drainage area of the Yangtze River and its tributaries (Fig. 1). The basement of the Yangtze Craton is dominated by Neoproterozoic rocks with sporadic outcrops of Archean rocks in the Kongling Terrane (Guo et al., 2014) and Zhongxiang (Zhou et al., 2015). The Kongling Terrane consists of Archean TTG-granitic gneisses and metasediments (Guo et al., 2014 and references therein) and it includes the oldest known rocks in South China which are granitic gneisses dated at 3.45 Ga. They have Hf model ages which vary from 3.6–3.9 Ga (Guo et al., 2014), reaffirming the existence of ca. 3.8 Ga old continental crust remnants in the Yangtze Craton (Zhang et al., 2006c). Crustal xenoliths from Paleozoic lamproite diatremes in the Yangtze Craton have zircon ages of 2.9–2.8 Ga and 2.6–2.5 Ga, implying widespread Archean basement to the Yangtze Craton (Zheng et al., 2006). Proterozoic 1.8–2.0 Ga metamorphism and magmatism was also widespread in South China (Zhang et al., 2006b), and there are voluminous late Mesoproterozoic to Neoproterozoic mafic to felsic volcanic and intrusive rocks, especially those with ages of 830–740 Ma, in the northern and northwestern part of the Yangtze Craton (Zhao and Zhou, 2008). Early Paleozoic granitoids, mostly dated at 435–470 Ma, are common in the eastern Yangtze Craton (Guan et al., 2014), and Mesozoic rocks, mainly exposed in the middle and lower reaches of the Yangtze River, are represented by Late Jurassic and Early Cretaceous granitoids and gabbros (Xie et al., 2011). Early Cretaceous volcanic rocks dominated by rhyolite and dacite, and subordinate basalt and basaltic andesite, are also reported in this region (Xie et al., 2011).

The Yangtze River catchment covers the northern part of the Cathaysia Block (CB), where the basement is dominated by Neoproterozoic and minor Paleoproterozoic rocks (Zhao and Cawood, 2012). Detrital zircons from the Badu complex reveal four age groups of 3.7–3.6 Ga, 3.2–3.0 Ga, 2.7–2.6 Ga and ~2.5 Ga (Yu et al., 2012). Their Hf model ages suggest three major crustal growth periods at 2.5 Ga, 2.8 Ga and 3.5–3.3 Ga, as well as two minor periods at ~3.7 Ga and 4.0 Ga (Yu et al., 2012), indicating that Archean crust may have existed in the Cathaysia Block. Early Paleozoic granitoids are widespread (Li et al., 2010b and references therein), and Mesozoic magmatic rocks,

formed as a response to tectonic regime change from the continent-continent collision in the Early Mesozoic to the largely extensional setting in the Late Mesozoic, are abundant in the Cathaysia Block (Zhou et al., 2006).

3. Analytical methods

More than 10 mg of zircon was separated by conventional magnetic and heavy liquid methods for each sample. To minimize preferential selection, regardless of colour, size, shape, and transparency, zircons were selected and mounted along with fragments of zircon standards 91,500 (Wiedenbeck et al., 2004), Penglai (Li et al., 2010a), Temora (Black et al., 2004) and Plešovice (Sláma et al., 2008) on double-sided adhesive tapes, which were then cast in epoxy resin in 25 mm-diameter mounts. The mounts were then ground and polished to expose the centers of the zircon grains. All zircons were documented with optical photomicrographs using transmitted light (Fig. 2) to identify grains with inclusions and cracks to be avoided during subsequent in situ U–Pb, Lu–Hf and O analyses. Dilute HNO_3 and pure ethanol were used to clean the surface of the grain mounts in order to avoid surface Pb contamination before analysis.

3.1. CL imaging

Cathodoluminescence imaging (CL) was used to determine the internal structures of zircons and to help select optimum spots for in situ analysis. The imaging was done at the State Key Laboratory of Continental Dynamics, Xi'an, China, using a FEI Quanta 400 FEG high resolution emission field environmental scanning electron microscope connected to an Oxford INCA350 energy dispersive system (EDS) and a Gatan Mono CL3+ system. The working distance for the CL system was 8.4 mm, while the EDS used a spot size of 6.7 nm with an accelerating voltage of 10 kV.

3.2. Oxygen isotope analysis

Because LA–ICP–MS analysis results in relatively large pits, oxygen isotopes were analyzed by SIMS before U–Pb ages and Lu–Hf isotopes were determined by LA–ICP–MS and LA–MC–ICP–MS. Oxygen isotope ratios of detrital zircons from samples CJ02 and HJ02 (online supplementary Table 1) were determined using a double-focusing, multi-collector Cameca IMS 1270 SIMS at the University of Edinburgh in October 2008. Detailed operating conditions, instrumental correction and data processing procedures are as reported by Kemp et al. (2006). Zircon 91,500 was used as the primary standard to correct for instrumental mass fractionation (IMF). The standard zircons Penglai and Temora-2 were treated as unknown samples during the run, and they yielded average values of 5.13 ± 0.52‰ (2 SD, $n = 27$) and 8.00 ± 0.74‰ (2 SD, $n = 24$), respectively. These values are in agreement, within uncertainty, with the recommended values of 5.30 ± 0.10‰ (Li et al., 2010a) and 8.00–8.20‰ (Black et al., 2004), respectively.

Oxygen isotopic ratios of zircons from all the other sand samples and of additional zircons from CJ02 (online supplementary TabSle 2) were analyzed using a double-focusing, multi-collector Cameca SIMS 1280 ion microprobe at the Institute of Geology and Geophysics, Chinese Academy of Sciences, Beijing in June and October 2011. The Cs^+ primary ion beam was accelerated at 10 kV, with an intensity of ~2 nA, and rastered over a 10 μm distance. The spot size was about 20 μm. Isotopes ^{16}O and ^{18}O were collected simultaneously using two Faraday cups and a mass resolution of 2500. The instrumental mass fractionation factor (IMF) was corrected using standard zircon Penglai with a δ-$^{18}O_{VSMOW}$ value of 5.30 ± 0.10‰ (Li et al., 2010a). The reproducibility of standard zircon 91,500 was generally better than 0.24‰ (1 SD), and the internal precision of a single analysis for $^{18}O/^{16}O$ ratios was generally between 0.1‰ and 0.4‰ (2 SE). The standard zircon 91,500 treated as an unknown during this analysis session, gave an average δ^{18}O value
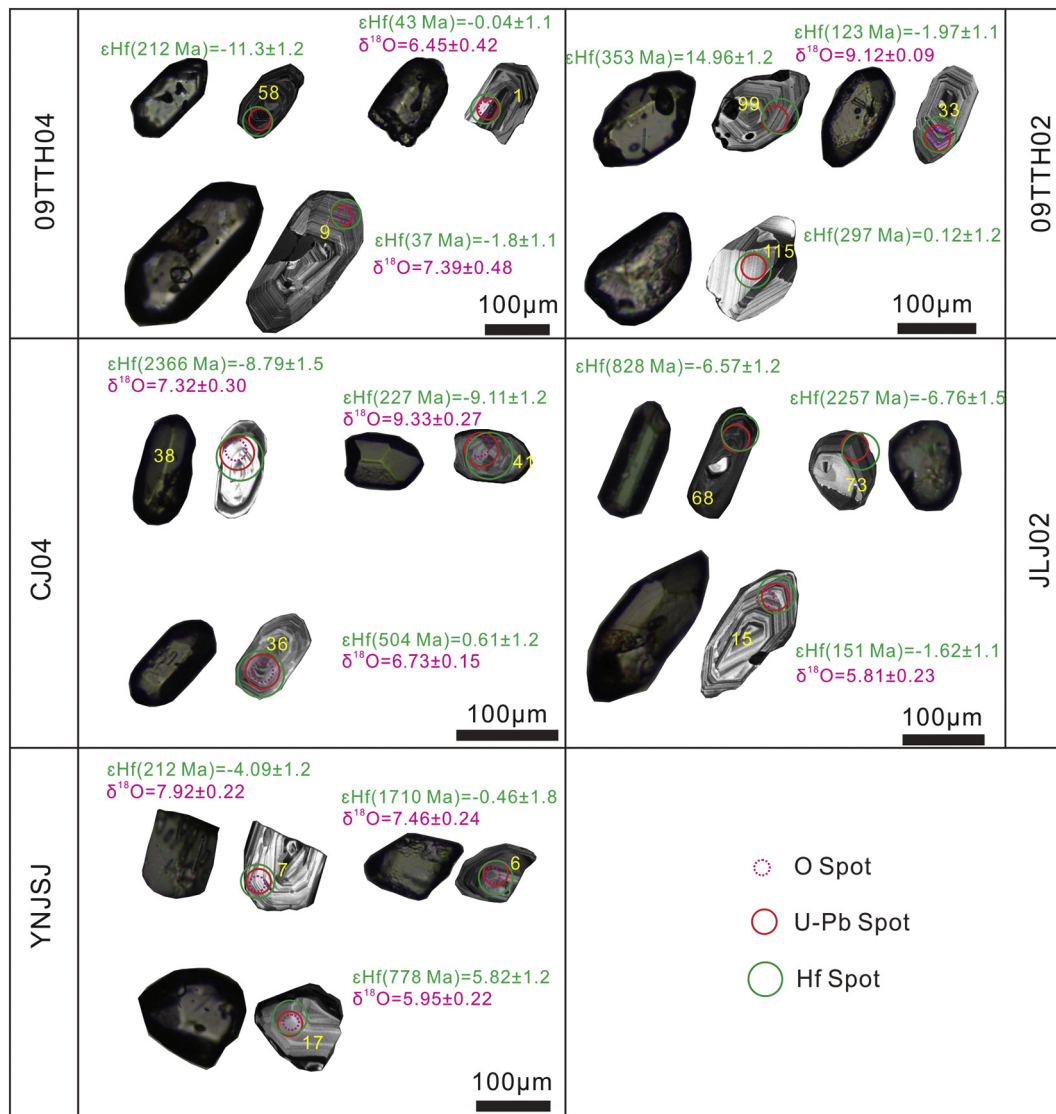
Fig. 2. Representative cathodoluminescence and transmitted light images for detrital zircons from the Yangtze River sediments.

of 10.29 ± 0.48‰ (2 SD, n = 42), which is consistent within analytical uncertainty with the recommended value of 9.94 ± 0.10‰ (Wiedenbeck et al., 2004). Detailed analytical techniques and data processing procedures were similar to those described by Li et al. (2010a).

3.3. U–Pb dating

U–Pb dating of all the detrital zircons (online supplementary Tables 1 and 2) was conducted by LA–ICP–MS at the State Key Laboratory of Geological Processes and Mineral Resources, China University of Geosciences, Wuhan. Laser sampling was performed using a GeoLas 2005 ArF excimer laser, with a wavelength of 193 nm and a pulse width of ~15 ns. An Agilent 7500a ICP–MS instrument was used to acquire ion-signal intensities. The diameter of the laser ablation craters was 32 μm with an energy density of 8 J/cm^2. The laser was fired at a frequency of 6 Hz. Helium was used as a carrier gas with a flow rate of 0.6 L/min. Argon was used as the make-up gas with a flow rate of 0.78 L/min and mixed with the carrier gas via a T-connector before introduction to the ICP. Nitrogen with a flow rate of 3 mL/min was added into the central gas flow of the Ar plasma to reduce the detection limit and improve sensitivity and precision (Hu et al., 2008). The

sampling depth was 5 mm, and this parameter together with the carrier and make-up gas flows were optimized by ablating NIST SRM 610 to obtain maximum signal intensity for ^{208}Pb, while keeping low ThO/Th and Ca^{2+}/Ca$^+$ ratios to minimize the matrix-induced interferences. The RF power is 1350 W. The plasma gas flow rate is 15 L/min, and the auxiliary gas flow rate is 1 L/min. Dwell times were set to be 10 ms for ^{232}Th, 15 ms for ^{238}U, ^{208}Pb and ^{204}Pb, 20 ms for ^{206}Pb and ^{207}Pb and 6 ms for ^{201}Hg. The detector mode is dual (pulse and analog). Each analysis consisted of background signals of 20–30 s and data signals of ca. 50 s.

The off-line selection and integration of background and analytic signals, and time-drift correction and quantitative calibration for U–Pb dating were performed by ICPMSDataCal (Liu et al., 2010). Common Pb correction was made following the method of Andersen (2002). The corrections are negligible in most cases. Zircon 91,500 was used as the external standard reference material for U–Pb dating. The standard reference zircons GJ-1 and Plešovice were treated as unknowns and they yielded average ^{206}Pb/^{238}U ages of 598 ± 17 Ma (2SD, n = 95) and 330 ± 13 Ma (2SD, n = 33), respectively, which are in agreement with the ID-TIMS ^{206}Pb/^{238}U age range of 599.8 ± 1.7 Ma for GJ-1 (Jackson et al., 2004) and 337.13 ± 0.37 Ma for Plešovice (Sláma et al., 2008).

3.4. Lu–Hf isotopic analysis

Only zircons with 90%–110% U–Pb age concordance were selected for Hf isotope analysis, and these were done in the same site, or in the same domain, where O isotope and U–Pb age determinations were measured.

Lu–Hf isotopes of zircons (online supplementary Table 1) analyzed for oxygen isotopic ratios at the University of Edinburgh were determined using a Nu Plasma HR MC–ICP–MS (Nu Instruments Ltd., UK), coupled to a GeoLas 2005 excimer ArF laser-ablation system hosted at the State Key Laboratory of Continental Dynamics, Northwest University, Xi'an. The laser energy density used was 15–20 J.cm^{-2}, with a spot size of laser beam was 44 μm in diameter and a pulse rate of 10 Hz. Helium was used as the carrier gas. The abundance sensitivity was 7–8 V per 1% for ^{180}Hf at 44 μm. Other detailed operating conditions and instrumental correction and data processing procedures are reported in Yang et al. (2009). The data quality was monitored by analyzing standard reference zircons GJ-1 and Temora-2, which yielded average values of 0.282014 ± 0.000059 (2 SD, n = 31) and 0.282660 ± 0.000063 (2 SD, n = 31), respectively. These values are in close agreement with the reported values of 0.282015 ± 0.000019 (2 SD, n = 25) for GJ-1 (Elhlou et al., 2006) and 0.282686 ± 0.000008 for Temora-2 (Woodhead et al., 2004).

Lu–Hf isotopes of all the other zircons (online supplementary Table 2) were analyzed on a Neptune Plus MC–ICP–MS (Thermo Fisher Scientific, Germany) coupled with a Geolas 2005 excimer ArF laser ablation system (Lambda Physik, Göttingen, Germany) at the State Key Laboratory of Geological Processes and Mineral Resources, China University of Geosciences, Wuhan. A combination of newly designed X skimmer cone and jet sample cone was used for the in situ Hf isotope analysis. The laser beam was 44 μm in diameter with an energy density of 5.3 J/cm^2 and a frequency of 8 Hz. A "wire" signal smoothing device was used in order to produce smooth signals (Hu et al., 2012a). Detailed operating conditions for the laser ablation system and the MC–ICP–MS instrument are described by Hu et al. (2012b).

A major difficulty in obtaining accurate in situ Hf isotopic compositions by LA–MC–ICP–MS is the isobaric interference from ^{176}Yb and ^{176}Lu on ^{176}Hf (Woodhead et al., 2004). The mass fractionations of Hf and Yb were calculated using values of 0.7325 for ^{179}Hf/^{177}Hf and 1.13017 for ^{173}Yb/^{171}Yb, respectively (Segal et al., 2003). The mass bias of Yb was used to calculate the mass fractionation of Lu due to their similar physicochemical properties. Interference of ^{176}Lu on ^{176}Hf was corrected by measuring the intensity of the interference-free ^{175}Lu isotope and using the recommended ^{176}Lu/^{175}Lu ratio of 0.02656 (Blichert-Toft et al., 1997); similarly, the ^{176}Yb interference was corrected using the measured intensity of interference-free ^{173}Yb and ^{176}Yb/^{173}Yb = 0.7938 (Segal et al., 2003). The off-line selection and integration of analytical signals, and mass bias calibrations were performed using ICPMSDataCal (Liu et al., 2010).

Time-drift correction and external calibration were determined using zircon standard 91,500. Our measured values of the standard reference zircons GJ-1 and Temora-2 as unknowns are 0.282018 ± 0.000027 (2 SD, n = 78) and 0.282687 ± 0.000030 (2 SD, n = 53), respectively, which are in good agreement with the recommended values of the previous studies (Elhlou et al., 2006; Woodhead et al., 2004).

In this study, the parameters and methods of calculation are as follows: the ^{176}Lu decay constant of 1.867×10^{-11} yr^{-1} (Scherer et al., 2001) and the recommended chondritic values of ^{176}Hf/^{177}Hf = 0.282785 and ^{176}Lu/^{177}Hf = 0.0336 (Bouvier et al., 2008) were adopted to calculate the single-stage model age, the two-stage model age and ε$_{Hf}$(t). Two-stage Hf model ages, T$_{DM2}$ and T$_{DM2}^{0.0115}$, were calculated. T$_{DM2}$ and T$_{DM2}^{0.0115}$ were calculated assuming that new crust was derived from a depleted mantle source with a present-day ^{176}Hf/^{177}Hf = 0.28325 and ^{176}Lu/^{177}Hf = 0.0384 (Griffin et al., 2002). The ^{176}Lu/^{177}Hf ratios of the source regions used to calculate T$_{DM2}$ were constrained by zircon grains of different ages with mantle-

like oxygen isotopes. For comparison, T$_{DM2}^{0.0115}$ shown in Fig. 8 assumes a mean crustal ^{176}Lu/^{177}Hf ratio of 0.0115 (Rudnick and Gao, 2003). The ε$_{Hf}$(t) is defined by parts per 10^4 deviation of ^{176}Hf/^{177}Hf between the sample value and the chondritic value, where t is the time when the zircon crystallized.

4. Results

4.1. U–Pb ages

In order to select the more reliable zircon ages we only consider zircon U–Pb ages with 90–110% concordance, following the approach by Amelin et al. (2000). Because of the low radiogenic ^{207}Pb content in young zircons, it can be difficult to obtain accurate ages, and so ^{207}Pb/^{206}Pb ages were adopted for zircons with ages of ≥1.0 Ga and ^{206}Pb/^{238}U ages for zircons with ages <1.0 Ga.

4.1.1. Tuotuo, Tongtian and Jinsha rivers

Sample 09TTH04 was collected from the Tuotuo River near the headwater (Fig. 1; Table 1). One hundred and twenty-six zircon grains were dated from this sample, of which 114 grains are concordant. These concordant zircons define two major age populations at 0–100 Ma with a peak at 41 Ma and 200–300 Ma, which make up 26.9% and 16.5% of the total concordant grains, respectively. There are also four smaller age groups at 400–500 Ma, 700–1000 Ma with two small peaks at 780 and 950 Ma, 1400–1500 Ma and 1800–1900 Ma, and two grains have ages of 2658 ± 17 Ma and 2629 ± 17 Ma (Fig. 3a, d).

Sample 09TTH02 is from the Tongtian River (Fig. 1; Table 1). One hundred and thirty-two concordant zircons out of 141 grains from this sample show three major age groups at 0–100 Ma with a peak at 41 Ma, 200–300 Ma and 400–500 Ma, with three smaller age groups at 700–1000 Ma, 1800–1900 Ma and 2400–2700 Ma. Thirteen grains younger than 100 Ma were identified comprising 10% of the concordant grains (Fig. 3b, e).

Sample YNJSJ was collected from the Jinsha River in Yunnan Province (Fig. 1; Table 1). This sample had 106 concordant zircons out of 117 grains, they show one major age group at 700–900 Ma, a diffuse group at 1.8–2.0 Ga and three restricted groups at 0–100 Ma, 200–300 Ma and 400–500 Ma. Only five grains have ages younger than 100 Ma, accounting for <7% of the total dated grains. One zircon has an age of 3128 ± 33 Ma (Fig. 3c, f).
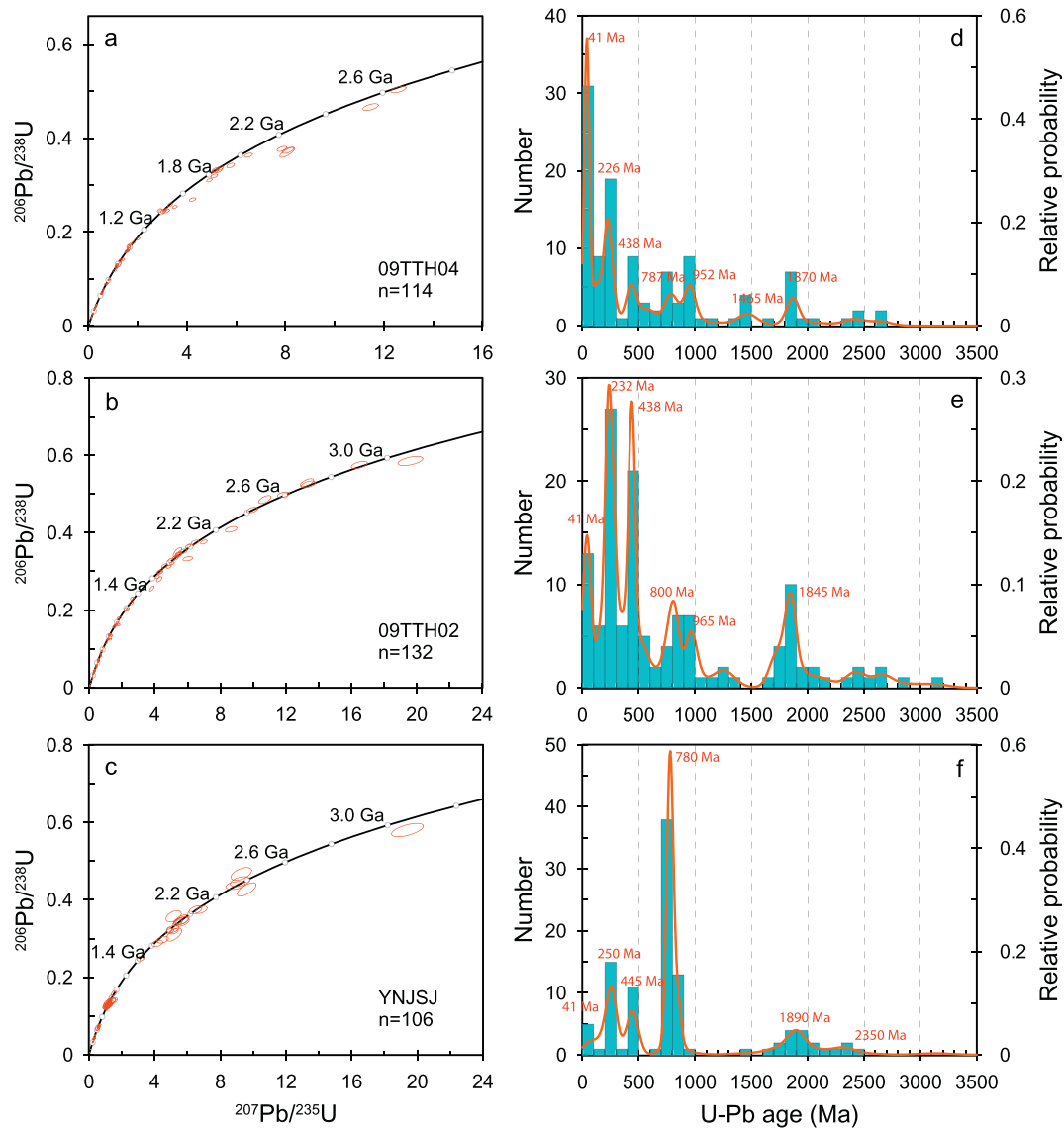
4.1.2. Yangtze River

Three samples were collected from the Yangtze River. Sample CJ04 is from the upper reaches at Chongqing (Fig. 1; Table 1). Fifty-six zircon grains were dated, of which forty-five grains are concordant. The concordant zircons define a distinct population at 700–900 Ma, which accounts for 40% of the zircons, with four smaller age groups at 100–300 Ma, 400–550 Ma, 1700–1800 Ma and 2400–2500 Ma (Fig. 4a, d).

Sample CJ02 was taken from the middle reaches at Wuhan (Fig. 1; Table 1). One hundred and forty-five zircons were dated from this sample, of which one hundred and sixteen grains are concordant. The concordant zircons define two major groups at 100–300 Ma with a peak at ~130 Ma and 600–900 Ma, with three smaller groups at 400–500 Ma, 1800–2000 Ma and 2400–2500 Ma (Fig. 4b, e).

Sample CJ07 was taken at the mouth of the Yangtze River at Shanghai (Fig. 1; Table 1). One hundred and nine concordant zircons out of a total of 130 grains have two major age groups at 100–300 Ma and 700–900 Ma. In addition, there is one 1.3 Ga zircon and four 1.7–2.4 Ga zircons (Fig. 4c, f).

4.1.3. Jialing River

Sample JLJ02 was collected at the confluence of the Jialing River with the Yangtze River at Chongqing (Fig. 1; Table 1). It contains significantly more Archean and Paleoproterozoic zircons than the other samples. One hundred and eight concordant zircons out of 127 grains dated

Fig. 3. U–Pb concordia plots (a, b, c) illustrating the U–Pb ages of detrital zircons from the upper Yangtze River. The corresponding age distributions are shown in the right panel (d, e, f), where the density curves are based on the Kernel Density Estimation (Vermeesch, 2012).

from this sample exhibit five age groups at 100–300 Ma with two small peaks at ~180 and 250 Ma, ~400–500 Ma, 700–900 Ma, 1800–2000 Ma with a peak at ca.1.9 Ga and 2400–2600 Ma. One zircon has an age of 3158 ± 41 Ma (Fig. 5a, e).

4.1.4. Han River

Two samples were collected along the Han River. Sample HJ02 was taken at the end of the middle reach at Zhongxiang (Fig. 1; Table 1), seventy zircon grains were dated from this sample, of which sixty-two grains are concordant. These concordant grains exhibit three major age populations at 100–300 Ma with a peak at 205 Ma, 400–500 Ma and 700–800 Ma. Four Paleoproterozoic zircons ranging in age from 1700 to 2400 Ma are also present (Fig. 5c, g).

The second sample, HJ01, was collected at the confluence of the Han River with the Yangtze River at Wuhan (Fig. 1; Table 1), and it yielded 112 concordant grains out of 122 zircons dated. They define three prominent age groups at 100–300 Ma with a peak at 210 Ma, 400–500 Ma with a peak at 446 Ma and 700–900 Ma. Four zircons are older than 1.5 Ga (Fig. 5b, f).

In summary, sample 09TTH04, 09TTH02 and YNJSJ are from the upper reaches of the Yangtze River, and remaining samples are from

the middle and lower reaches of the Yangtze River. Zircons from the upper Yangtze River have age groups at 0–100 Ma, 200–300 Ma, 400–500 Ma, 700–1000 Ma, 1800–1900 Ma and 2300–2500 Ma. There is a striking peak at 41 Ma on samples from the uppermost reaches diagnostic of igneous rocks on the Tibetan Plateau, whereas those from the middle and lower Yangtze River and its tributaries exhibit broadly similar age groups at 100–300 Ma, 400–500 Ma, 700–900 Ma, 1800–2000 Ma and 2300–2700 Ma, except that they lack Cenozoic zircons (Fig. 5d, h).

4.2. Oxygen isotopes

Oxygen isotopic compositions of zircons are often divided into three groups: mantle-like (4.7–6.0‰; Spencer et al., 2014), and those with $\delta^{18}O < 4.7‰$ and $> 6.0‰$, respectively. The results for the concordant zircons in the different samples are plotted in Fig. 6, 510 zircons were analyzed for O isotopes, of which 448 zircons are concordant. Of the concordant zircons, ~23% ($n = 104$) have mantle-like $\delta^{18}O$ values and 70% ($n = 314$) and ~7% ($n = 31$) have higher and lower $\delta^{18}O$ values, respectively, The concordant and discordant zircons have similar $\delta^{18}O$ distributions (Fig. 6j).
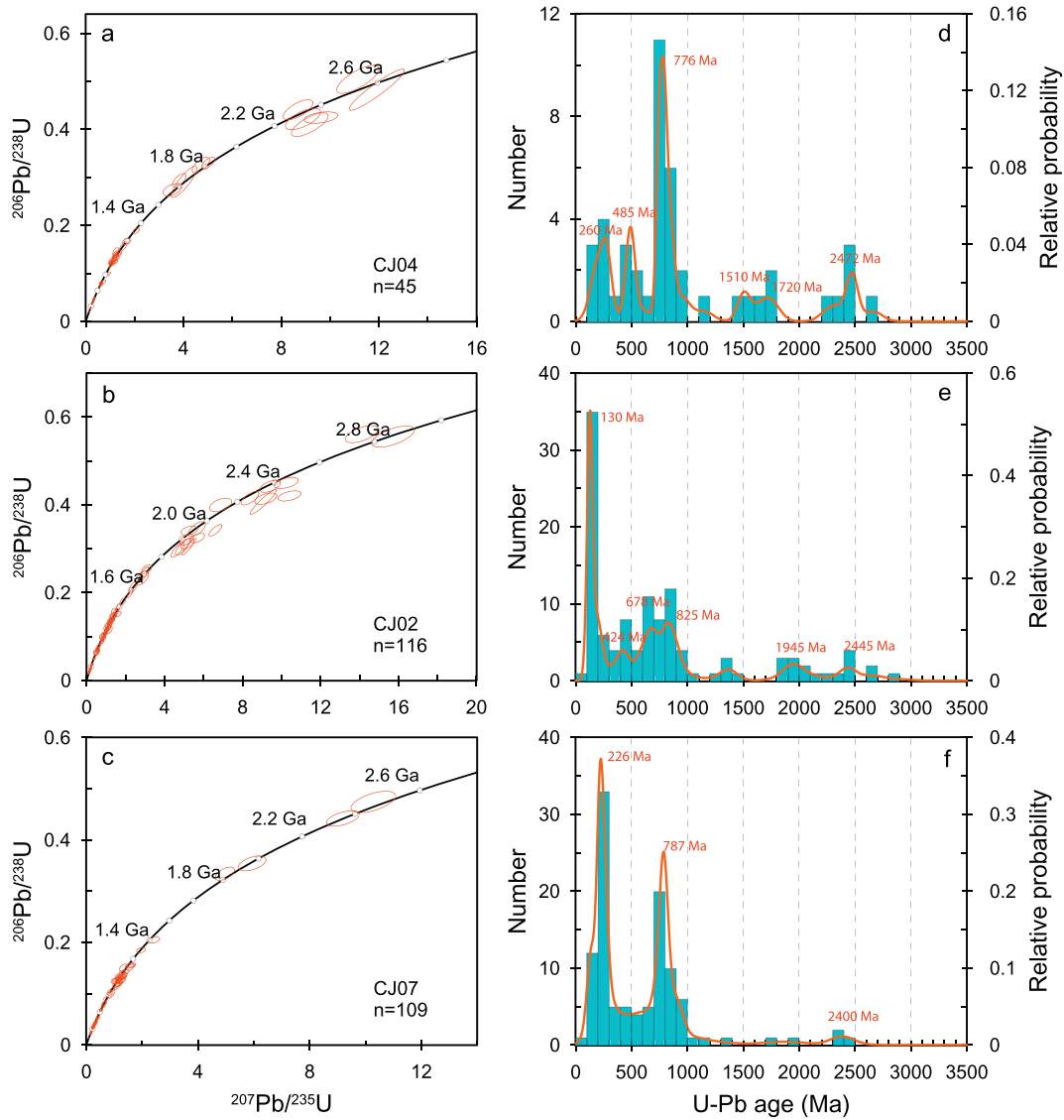
Fig. 4. U–Pb concordia plots (a, b, c) illustrating the U–Pb ages of detrital zircons from the middle and lower Yangtze River. The corresponding age distributions are shown in the right panel (d, e, f), where the density curves are based on the Kernel Density Estimation (Vermeesch, 2012).

4.3. Hf isotopes

The Hf isotope ratios are summarized in Fig. 7. The range in ε_{Hf}(t) tends to increase as the crystallization ages of the zircons decrease. Zircons older than 2.4 Ga have a relatively small range in ε_{Hf}(t) between −8 and +8, except for one grain with a value of ca. −12. The Paleo- and Mesoproterozoic zircons are characterized by negative ε_{Hf}(t) values, and they show a slightly broader range of ε_{Hf}(t) from −12 to +12. Zircons dated at 100–300 Ma and 700–900 Ma have similar distribution patterns in ε_{Hf}(t) ranging from highly negative to coeval depleted mantle values (ca. −32 to +16). In contrast, the 400–500 Ma zircons exhibit a small range from ca. −10 to +12. The youngest zircon population displays a narrow range from ca. −3 to +3 (Fig. 7j).

5. Discussion

5.1. Distribution of U–Pb crystallization ages

Zircons from the upper, middle and lower reaches of the Yangtze River define six age groups at 0–100 Ma with a striking peak at ca. 41

Ma, 200–300 Ma, 400–500 Ma, 700–900 Ma, 1800–2000 Ma and 2400–2700 Ma. These are similar to the results of Iizuka et al. (2010) and He et al. (2013), except for the lack of a significant amount of Cenozoic zircons in the data of Iizuka et al. (2010). This presumably reflects the one sample from which zircons were analyzed, and that it was collected at Nanjing, in the lower reaches of the Yangtze River.

The Jialing River rises from the Western Qinling Orogen, flows across the Sichuan basin and joins the Yangtze River in Chongqing. The Han River originates from the South Qinling Orogen and joins the Yangtze River in Wuhan (Fig. 1). Both rivers drain entirely from within the Yangtze Craton, and the detrital zircons from the two rivers are sourced from the northern and northwestern part of the Yangtze Craton. As seen in Fig. 5, zircons from both Han and Jialing rivers have similar age populations with groups at 100–300 Ma, 400–500 Ma and 700–900 Ma, although the 400–500 Ma zircon population is not so well developed in the Jialing River. The zircons from the Han River have very few Paleoproterozoic and Archean zircons, in contrast to those from the Jialing River (Fig. 5). This may be because the Jialing River drains the Sichuan basin, which sampled old sediments formed by weathering and erosion of rocks around the basin.

Paleoproterozoic and Archean zircons account for only ~6% and 4% of all the zircons analyzed, reflecting the scarcity of outcrops of rocks of
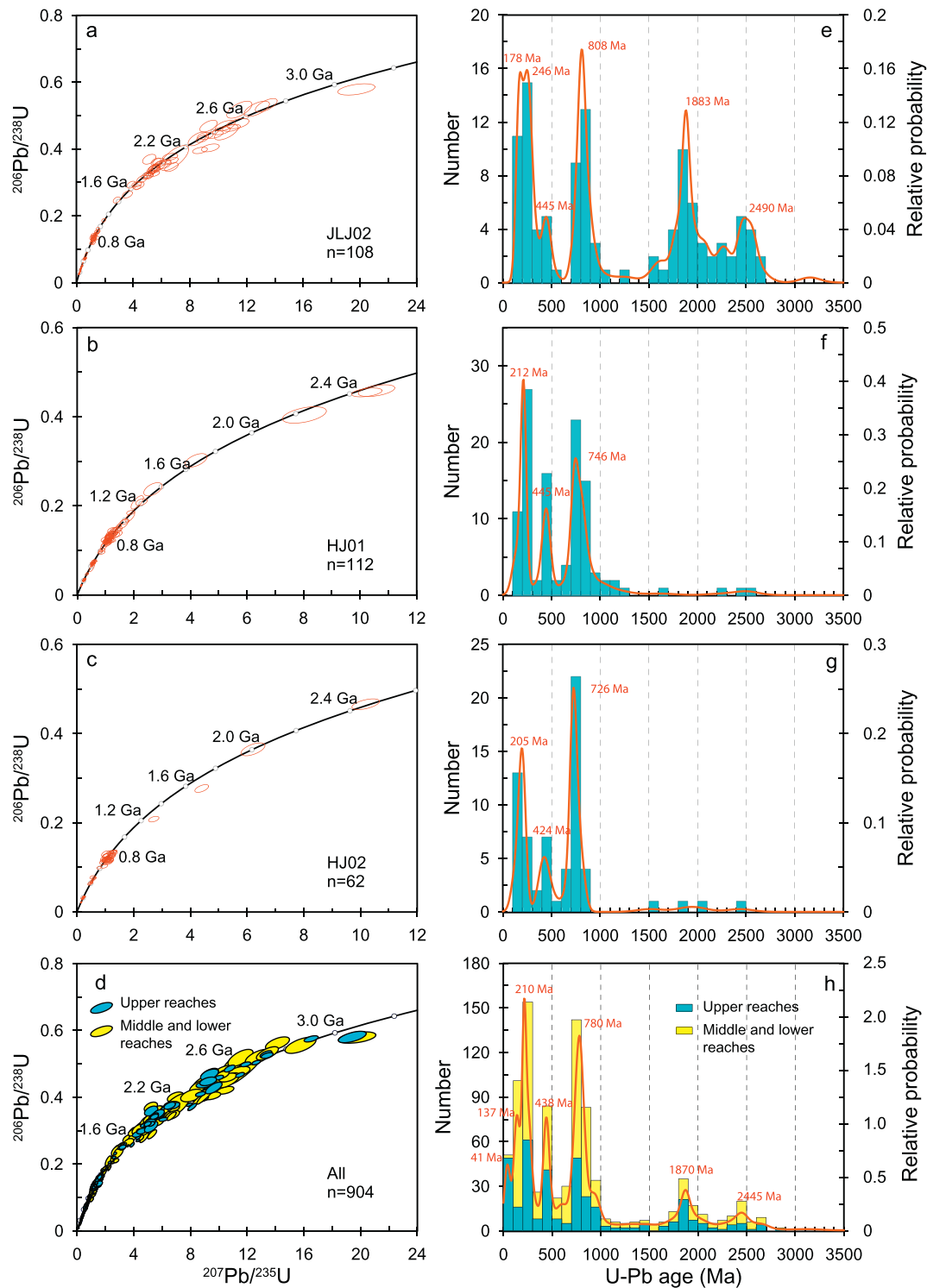
Fig. 5. U–Pb concordia plots (a, b, c) illustrating the U–Pb ages of detrital zircons from the Han and Jialing rivers and a plot of all the zircons analyzed in this study. The corresponding age distributions are shown in the right panel (e, f, g, h), where the density curves are based on the Kernel Density Estimation (Vermeesch, 2012). Samples 09TTH04, 09TTH02 and YNJSJ are from the upper reaches of the Yangtze River, and other six samples are from the middle and lower reaches of the Yangtze River.

these ages in the Yangtze Craton (e.g., Guo et al., 2014; Zhou et al., 2015). Nonetheless, the Archean-Paleoproterozoic zircons (2.4–2.7 Ga) have similar ages to the 2.5–2.6 Ga zircons from crustal xenoliths from lamproite diatremes (Zheng et al., 2006) and the ~2.5–2.6 Ga A-type granite in the Yangtze Craton (Zhou et al., 2015), reaffirming the widespread Archean basement underneath the Yangtze Craton (Zheng et al., 2006). The 1.8–2.0 Ga age group is similar in age to collisional and post-collisional events in the Yangtze Craton (Peng et al., 2012),

presumably resulting from the assembly of the Columbia supercontinent (Zhao et al., 2002).

All the river samples from the Yangtze Craton have a dominant population at 700–900 Ma, which matches well with the ages of widespread mid-Neoproterozoic magmatism along the western, northern, northwestern and southeastern margins of the Yangtze Craton (Zhao and Zhou, 2008, 2013). This magmatism is thought to be linked to the breakup of the Rodinia (Li et al., 2008 and references therein), although
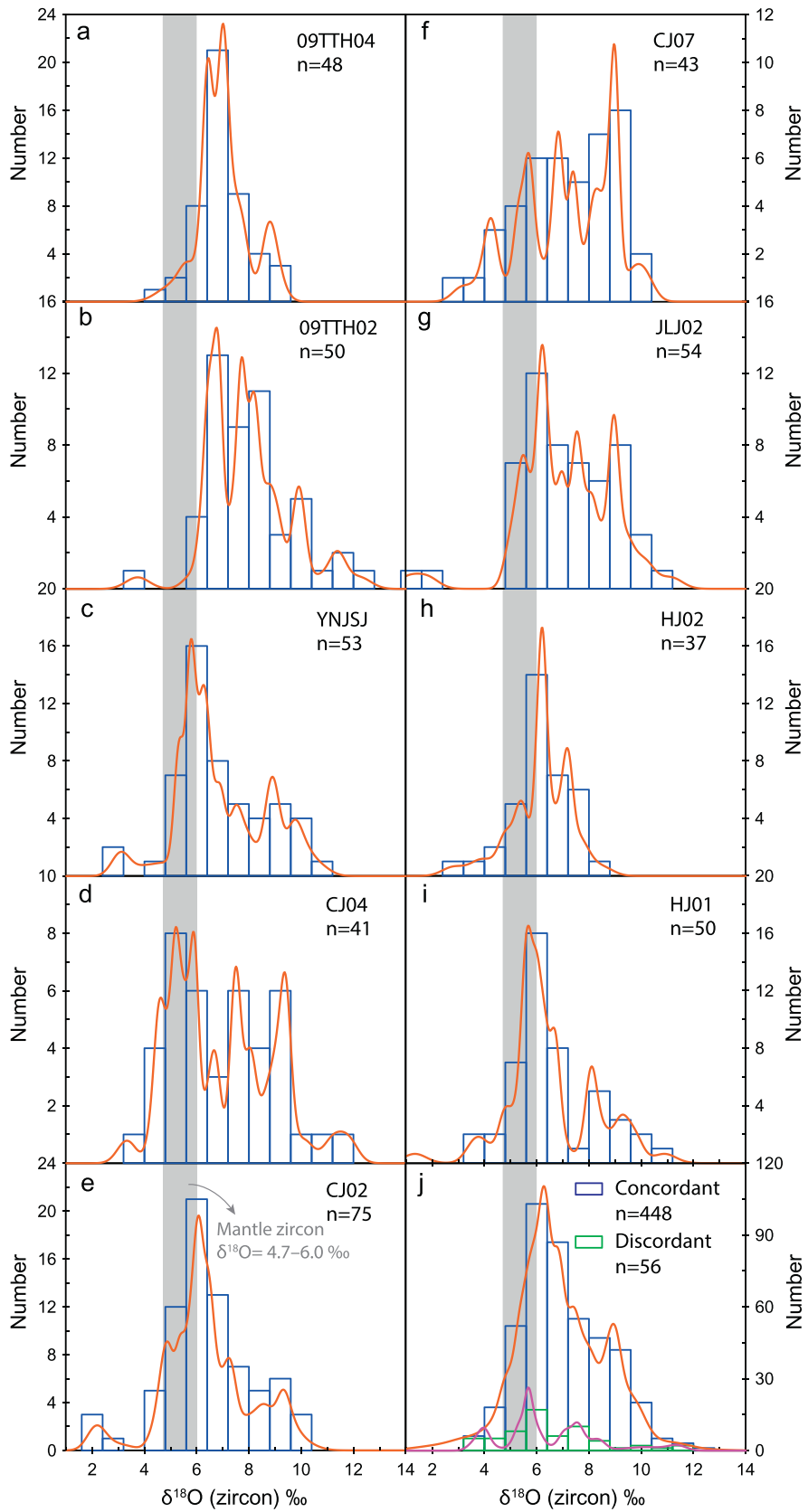
Fig. 6. Distribution of oxygen isotope δ^{18}O values in concordant zircons from the Yangtze River (a–f) and its tributaries, the Han and Jialing rivers (g–i), and in all the concordant and discordant zircons plotted together(j). The density curves are based on the Kernel Density Estimation (Vermeesch, 2012), and the grey bars show the range of zircons with mantle-like δ^{18}O of 4.7–6.0‰ (Spencer et al., 2014).
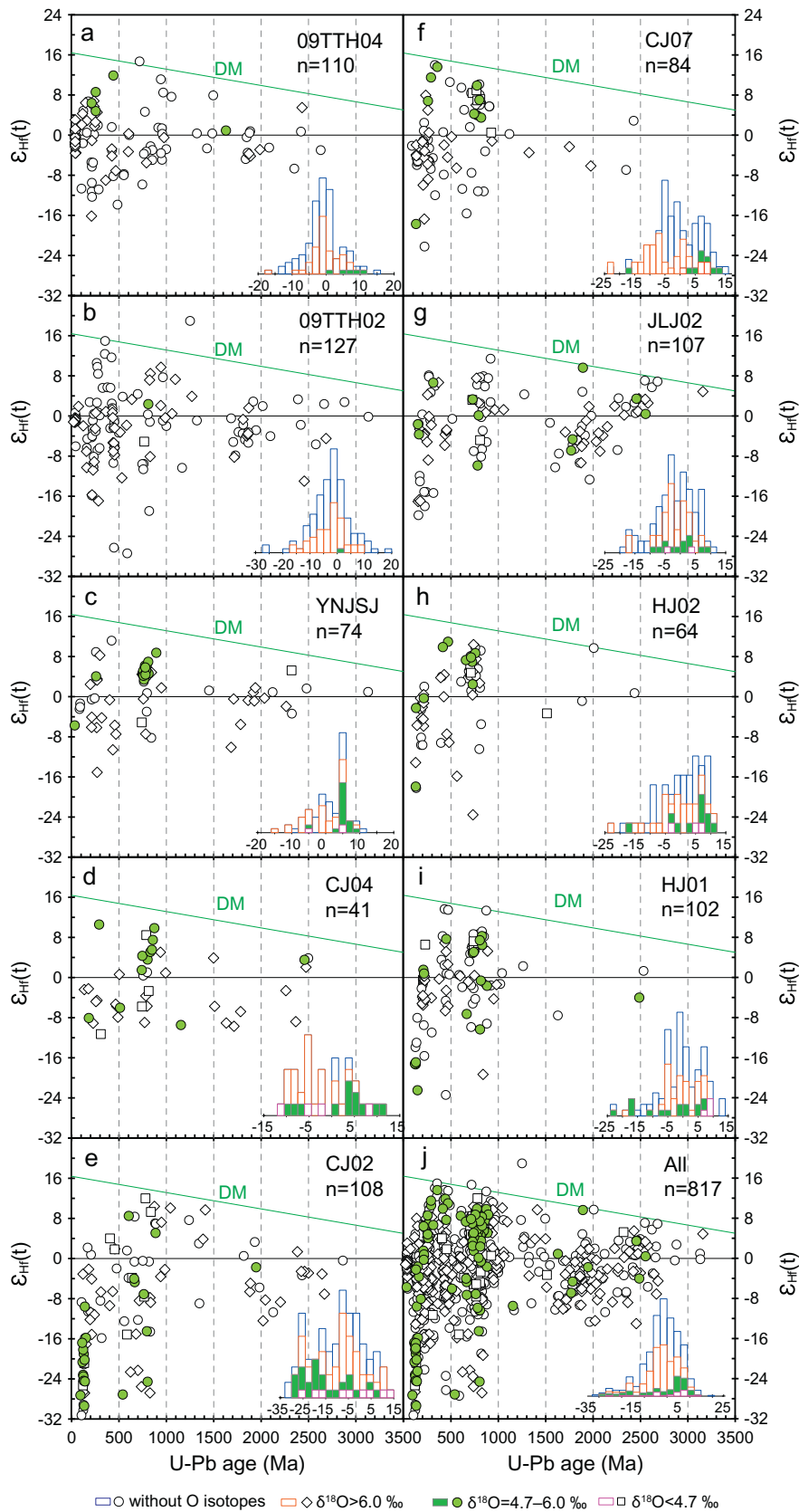
Fig. 7. Variations of ε$_{Hf}$(t) as a function of zircon crystallization ages for the detrital zircons from the Yangtze River (a–f), its tributaries the Han and Jialing rivers (g–i) and all the zircons analyzed for Hf isotopes plotted together (j). The green solid lines labeled DM indicate the evolution line of depleted mantle (Griffin et al., 2002). Insets show the distributions of ε$_{Hf}$(t).

it has also been associated with slab subduction during the amalgamation of the Yangtze Craton and Cathaysia Block (Zhao and Zhou, 2013).

Early Paleozoic zircons occur in all the samples analyzed. These zircons cluster in a prominent age group at 400–500 Ma, corresponding to an Early Paleozoic intraplate orogenic event in South China (Guan et al., 2014; Li et al., 2010b). The felsic intrusions in the intraplate orogen are dominated by S-type granites (Guan et al., 2014), and so most of these zircon grains have negative $\varepsilon_{Hf}(t)$ down to values of -10 (Fig. 7). In the South Qinling Belt, the Early Paleozoic magmatic belt is mainly composed of intermediate and mafic magmatic rocks, which are thought to represent a significant phase of crustal extension in the northern margin of the Yangtze Craton (Wang et al., 2017). These rocks may be the source of zircons with positive $\varepsilon_{Hf}(t)$ values from the Han River (Fig. 7h, i).

As stated above, the late Paleozoic and Mesozoic zircons from the upper reaches of the Yangtze River cluster at 200–300 Ma with an age peak at ~230 Ma, whereas those grains from the middle and lower reaches have an age group at 100–300 Ma (Fig. 5d, h). Early Mesozoic granitoids dominated by middle to late Triassic post-collisional granites are widely distributed in the Qiangtang Terrane (Chen et al., 2016). These rocks have ages ranging from ca. 240 to 210 Ma (Chen et al., 2016; Peng et al., 2015), marking the final closure of the Paleo-Tethys Ocean and associated continent–continent collision between the Southern and Northern Qiangtang terranes. The age peak at ~230 Ma from the upper reaches appears to reflect the igneous rocks associated with this collisional event.

Early Mesozoic granitoids are also widespread in the South Qinling Belt (Sun et al., 2002), including the 235–250 Ma granitoids mainly exposed in the western part of the West Qinling (Zeng et al., 2014), and slightly younger rocks with ages of 205–220 Ma, attributed to collision between the North China and Yangtze cratons in the Triassic (Sun et al., 2002). A few scattered Late Mesozoic granitoids (170–100 Ma) are also exposed in this region (Wang et al., 2013), consistent with the Mesozoic age population in the detrital zircons from the Yangtze River. The Tuotuo River originates and flows through the Qiangtang Terrane (Fig. 1), where Cenozoic volcanic rocks with ages between 65 and 26 Ma are widespread (Xia et al., 2011). This explains why the 0–100 Ma zircons dominate the zircon ages in sample 09TTH04 from the Tuotuo River (Fig. 3). Zircons from the Tongtian River have similar age populations to those in the Tuotuo River, except for the difference in the proportion of each age group (Fig. 3). The greater proportions of 200–300, 400–500 and 1800–1900 Ma age populations, together with fewer Cenozoic zircons, is probably due to contributions from sediments eroded along the mainstream in the Songpan–Ganze upstream of sample 09TTH02.

The 0–100 Ma zircons in the Tuotuo River sample have a prominent age peak at 41 Ma, corresponding to magmatism associated with the collision between the Indian and Asian plates (Xia et al., 2011 and references therein). This is only found in the uppermost reaches, and the proportion of these zircons exponentially decreases, downstream, along the Yangtze River. The 41 Ma peak has completely disappeared somewhere upstream of Chongqing, where the detrital zircons are dominated by zircons from older sources carried by the tributaries in the downstream region.

5.2. Crustal growth and evolution of the main tectonic units within the drainage area

As discussed in Section 2, the Yangtze River catchment covers five tectonic units, including the Northern Qiangtang Terrane, the Songpan–Ganze Fold Belt, the South Qinling–Dabie Orogenic Belt, the Yangtze Craton and the Cathaysia Block (Fig. 1). U–Pb–Hf isotopic compositions for zircons from one river sand sample collected in the lower reaches of the Yangtze River, and from ten samples along the Yangtze River and its tributaries have been reported by Iizuka et al. (2010) and He et al. (2013). He et al. (2013) also estimated the crustal growth

rates of the upper, middle and lower segments of the Yangtze drainage area.

It is widely accepted that zircon crystallization involves at least a two-stage process (e.g. Campbell and Hill (1988)): (i) extraction of mafic magma from the mantle by partial melting; (ii) remelting of the protocrust to form felsic magma, from which most zircons crystallize. Hf two-stage depleted mantle model ages ($T_{DM2}^{0.0115}$) were therefore calculated for all zircons assuming an average continental crust $^{176}Lu/^{177}Hf$ ratio of 0.0115 (Rudnick and Gao, 2003) for the source regions of the magmas from which the zircons crystallized (Griffin et al., 2002). Fig. 8 illustrates the distribution of Hf model ages ($T_{DM}^{0.0115}$) for zircons from samples collected from river locations situated in the different tectonic units.

The Qiangtang Terrane, in the central to north of the Tibetan Plateau, has received increasing attention, although its record of crustal growth and evolution is still not clear. Sample 09TTH04 was collected close to the headwater in the Qiangtang Terrane (Fig. 1), and so it offers some new constraints. The crustal model ages have two major groups at 0.9–1.1 Ga and 1.7–1.8 Ga, and a small one at 2.6–2.7 Ga (Fig. 8a). The two major age groups are similar to the Hf two-stage model ages ($T_{DM}^{0.0115}$), clustered at 0.8–1.0 Ga and 1.6–1.9 Ga, for zircons from the Triassic granitoids and volcanic rocks in the Northern Qiangtang Terrane (Peng et al., 2015 and references therein). The small age population at 2.6–2.7 Ga indicates that the crustal growth in the Qiangtang Terrane started in the Late Archaean.

The evolution of the Songpan–Ganze Fold Belt can now be constrained from the crust formation ages of zircons from sample 09TTH02. In Fig. 8b these are compared with the model ages for detrital zircons from Triassic sediments that overlie this belt (Zhang et al., 2014). The results of Zhang et al. (2014) and those presented here have similar Hf model ages spectra with a wide range of model ages at 0.9–1.8 Ga and 2.5–2.8 Ga, together with a small peak at 2.0–2.1 Ga. However, these ages should be treated cautiously when considering the growth and evolution of the SGFB, as the provenance of these Triassic sediments is still a matter of debate. For example, sources in the North China Craton appear also to have made a minor contribution to these Triassic sediments (Bruguier et al., 1997; Weislogel et al., 2006).

The South Qinling–Dabie Orogenic Belt, is traditionally considered to belong to the North margin of the Yangtze Craton (e.g., Chen and Jahn, 1998; Dong et al., 2011). The Han River and the Jialing River, originating from the South Qinling–Dabie Orogen, drain entirely within the Yangtze Craton (Fig. 1) and so the South Qinling–Dabie Orogenic Belt is included as a part of the Yangtze Craton in the discussion of models of crustal growth.

The Yangtze Craton occurs across most of the catchment area. Our samples collected within the Yangtze Craton were therefore used to evaluate its crustal growth and evolution. The crust formation ages from our zircons indicate two episodes of crustal growth in South China, one broad period of 1.0–1.8 Ga with a peak at 1.0–1.4 Ga, and a period with fewer zircons at 2.5–2.9 Ga (Fig. 8c), similar to the results of Iizuka et al. (2010) and He et al. (2013). The major growth period in the Paleo- to Mesoproterozoic (1.0–2.0 Ga) is also observed in the compilation of Nd model ages from different rock types in the Yangtze Craton, which highlights that the Paleo- to Mesoproterozoic was a significant period in the growth and evolution of the Yangtze Craton (Chen and Jahn, 1998).

For comparison, we also calculated the crustal model ages of the Northern Cathaysia Block based on U–Pb–Hf isotopic data for zircons from Li et al. (2012) and He et al. (2013). Unlike that of the Yangtze Craton, the distribution of crustal model ages reveals three major episodes at 0.5–1.2, 1.3–1.8 and 2.0–2.5 Ga, with four small groups at 2.7–2.8, 2.9–3.0, 3.1–3.2 and 3.4–3.5 Ga (Fig. 8d). Compilation of Nd model ages from granitoids, volcano-sedimentary and clastic sedimentary rock centers on a broad peak at ca.1.6–2.7 Ga (Chen and Jahn, 1998), consistent with the two major periods of crustal model ages based on detrital zircons from Li et al. (2012) and He et al. (2013). Crustal
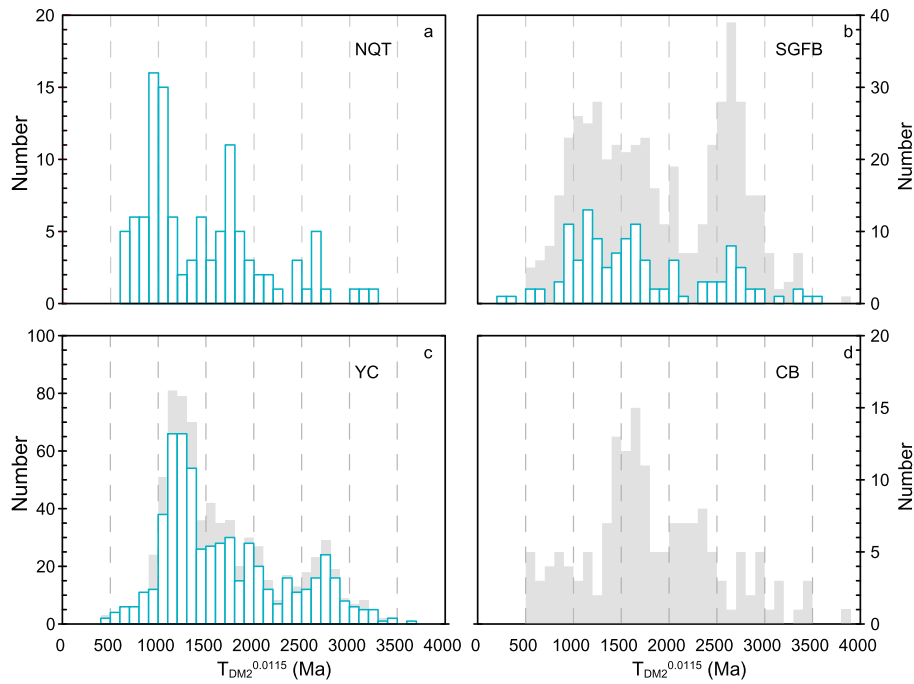
Fig. 8. Histogram of the crust model ages ($T_{DM}^{0.0115}$) for all the detrital zircons calculated assuming an average crustal $^{176}Lu/^{177}Hf$ ratio of 0.0115 (Rudnick and Gao, 2003). NQT = Northern Qiangtang Terrane; SGFB = Songpan–Ganze Fold Belt; YC = Yangtze Craton; NCB = Northern Cathaysia Block. Data sources: blue histogram in (a, b, c), this study; grey filled area in (b) from Zhang et al. (2014); grey filled area in (c) from Iizuka et al. (2010). Data sources in (d) are from Li et al. (2012) and He et al. (2013).

model ages from both detrital zircons and Nd isotope ratios of different rock types indicate that much of the Cathaysia Block was formed during the Paleo- to Mesoproterozoic.

5.3. Crustal growth periods based on zircons with constraints from oxygen isotopes

Zircon two-stage Hf model ages are used to constrain the periods of crustal growth. However, such ages may be the result of mixing if the parental magmas incorporate reworked material from different source terrains and hence contain ambiguous geological information (Hawkesworth and Kemp, 2006). Oxygen isotope data have therefore been used to screen out zircons with elevated $\delta^{18}O$ values that are more likely to contain recycled sedimentary material (Hawkesworth and Kemp, 2006; Kemp et al., 2006; Valley et al., 2005).

Hf depleted mantle model ages are sensitive to the selected $^{176}Lu/^{177}Hf$ ratio of the crustal source rocks. Such model ages may, for example, be up to 500 Ma older if the $^{176}Lu/^{177}Hf$ ratio of mafic crust is used rather than that of upper continental crust (Wang et al., 2009). To minimize the uncertainties of Hf crustal formation ages, we have tried to constrain the crustal-source $^{176}Lu/^{177}Hf$ ratios from $\varepsilon_{Hf}(t)$-age arrays defined by zircons with mantle-like $\delta^{18}O$ values (e.g., Hawkesworth et al., 2010; Kemp et al., 2006).

Zircons with mantle-like $\delta^{18}O$ values from the Yangtze River and its tributaries define five linear arrays (Fig. 9). The first three and the last array yield $^{176}Lu/^{177}Hf = 0.020–0.025$, which is in the range for mafic crust ($^{176}Lu/^{177}Hf = 0.019–0.028$; Amelin et al., 1999; Hawkesworth et al., 2010). However, the fourth array yields $^{176}Lu/^{177}Hf = 0.016$, similar to the values for the middle continental crust ($^{176}Lu/^{177}Hf = 0.013$; Rudnick and Gao, 2003).

To make the calculation simple and clear, the model ages have been calculated using crustal-source $^{176}Lu/^{177}Hf$ ratios of 0.020 obtained from Fig. 9 for all the zircons with mantle-like $\delta^{18}O$ values, and upper crustal $^{176}Lu/^{177}Hf$ ratios of 0.0083 for zircons with elevated $\delta^{18}O$. Fig. 10 shows the distribution of crustal formation ages based on two-stage Hf model ages for zircons for which oxygen isotope analyses are
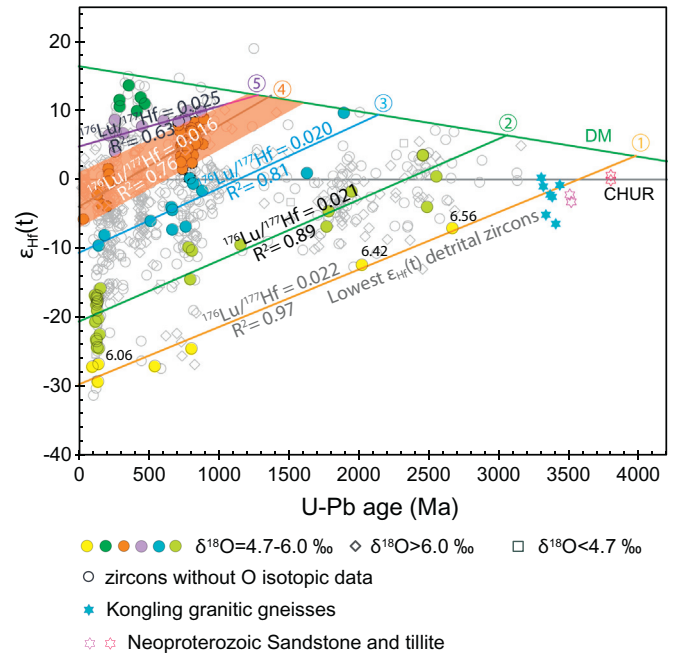
Fig. 9. Variations of $\varepsilon_{Hf}(t)$ against U–Pb crystallization ages of detrital zircons from the Yangtze River and its tributaries, the Han and Jialing rivers. The thick solid lines labeled DM and CHUR indicate evolution lines of depleted mantle (Griffin et al., 2002) and chondritic uniform reservoir, respectively. Other solid lines denote arrays defined by detrital zircons with mantle-like $\delta^{18}O$ (4.7–6.0‰) (filled circles) with derived $^{176}Lu/^{177}Hf$ ratios and correlation coefficients (R^2). Regression of the array with the lowest $\varepsilon_{Hf}(t)$ also includes three zircons with $\delta^{18}O$ of 6.06–6.56‰. Smaller open diamonds, open squares and open circles indicate detrital zircons with $\delta^{18}O > 6.0‰$, $\delta^{18}O < 4.7‰$ and without O isotopic data, respectively. Filled blue stars represent the 3.3–3.45 Ga magmatic zircons with mantle-like $\delta^{18}O$ values from granitic gneisses in the Kongling Terrane (Guo et al., 2014). Open red stars indicate the ~3.5 and 3.8 Ga detrital zircons from Neoproterozoic tillite and sandstone in the northern Yangtze craton (Liu et al., 2008; Zhang et al., 2006c).

available. Zircons with mantle-like and crustal-like oxygen isotopic values have different model age distributions, highlighting that the model ages of samples that may contain contributions from sedimentary material tend to be more variable. The T_{DM2} of mantle-like zircons clearly shows two major crustal growth periods at 1.4–1.6 Ga with a peak at ca. 1.5 Ga, and 2.8–3.0 Ga with a peak at ca. 2.9 Ga (Fig. 10). In contrast, zircons with elevated $\delta^{18}O$ values have two broad peaks in the range 0.8–1.8 Ga, with small peaks at ca. 0.9 Ga, ca.1.1 Ga, 1.2 Ga, 1.5 Ga and 2.3–2.8 Ga (Fig. 10).

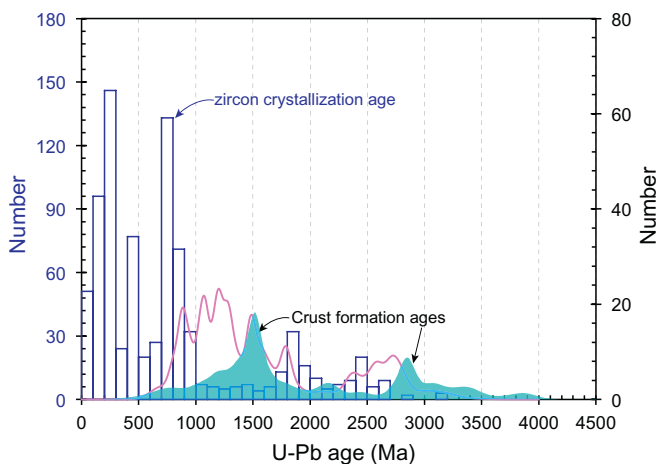### 5.4. Crust generation curves of South China and global comparison

The Yangtze drainage area is covered by thick Phanerozoic sedimentary rocks. Exposed Archean rocks are confined to a very small area of 360 km^2 (Guo et al., 2014) at Yichang (Fig. 1). This accounts for <0.02% of the total drainage area, even though much of the drainage basin is underlain by Archean crust (Liu et al., 2008; Zheng et al., 2006). Thus in any study that seeks to sample bulk crustal compositions Archean zircons will be under-represented in the modern river sand samples (Cawood et al., 2013). To overcome this problem, we apply the approach of Dhuime et al. (2012). We refer to the Hf model ages of zircons with $\delta^{18}O = 4.7$–6.0‰ and $\delta^{18}O > 6.0$‰ as new crust formation ages and hybrid model ages, respectively. We then estimate proportions of new crust formation ages through time by using the number of zircons with $\delta^{18}O = 4.7$–6.0‰ relative to the total number of zircons with $\delta^{18}O > 4.7$‰. The proportions are calculated in 100 Ma time intervals based on detrital zircons with oxygen isotope data from this study (online supplementary Tables 1 and 2), as well as zircons with oxygen isotope data from volcaniclastic and clastic sedimentary rocks (Wang et al., 2011), middle to late Permian sediments (Li et al., 2012) from South China and two Neoproterozoic sedimentary rocks LT07 and GCH01 (Table 1) in the northern Yangtze Craton (X. M. Liu's paper in preparation for submission) (Fig. 11a). Following Dhuime et al. (2012) we then apply the obtained proportions of new crust formation ages to all the available detrital zircons with Hf isotopes in South China (He et al., 2013; Iizuka et al., 2010; Li et al., 2012; Liu et al., 2008; Wang et al., 2011) to calculate the distributions of new and reworked crust and the variations in the rates of reworking of the

Fig. 10. Histogram of crystallization ages of detrital zircons, with the number shown on the left vertical axis, from the Yangtze River and its tributaries, the Han and Jialing rivers. Also shown are distributions of crust formation ages of zircons with mantle-like (4.7–6.0‰) (blue filled area), hybrid (> 6.0‰) (pink solid curve) $\delta^{18}O$, and the number of these zircons is shown on the right vertical axis. Crust formation ages, calculated using crustal-source $^{176}Lu/^{177}Hf$ ratio of 0.020 obtained from Fig. 9 for all the zircons with mantle-like $\delta^{18}O$ values, and upper crustal $^{176}Lu/^{177}Hf$ ratios of 0.0083 for zircons with elevated $\delta^{18}O$, are based on two-stage depleted mantle (T_{DM2}) model ages. For all the data plotted the 'number' of detrital zircons is that within a time interval of 100 Ma.

continental crust in South China through time (Fig. 11b). This then is the basis for the derivation of continental crustal growth curves for South China (Fig. 11c). The variations of the reworked crust through time is given by the distribution of the crystallization ages of zircons with Hf model ages much older than their crystallization ages. In this way, the bias of the geological record toward the younger material is to some degree circumvented. However, it should also be noted that crustal growth curves calculated using the method by Dhuime et al. (2012) are minimal estimates, both because some crust is thought to be rapidly recycled such that it does not leave an isotopic record (cf. Armstrong and Harmon, 1981), and because zircons tend to crystallize from relatively evolved magmas and so more mafic crust may be under-represented (Cawood et al., 2013; Hawkesworth et al., 2018).
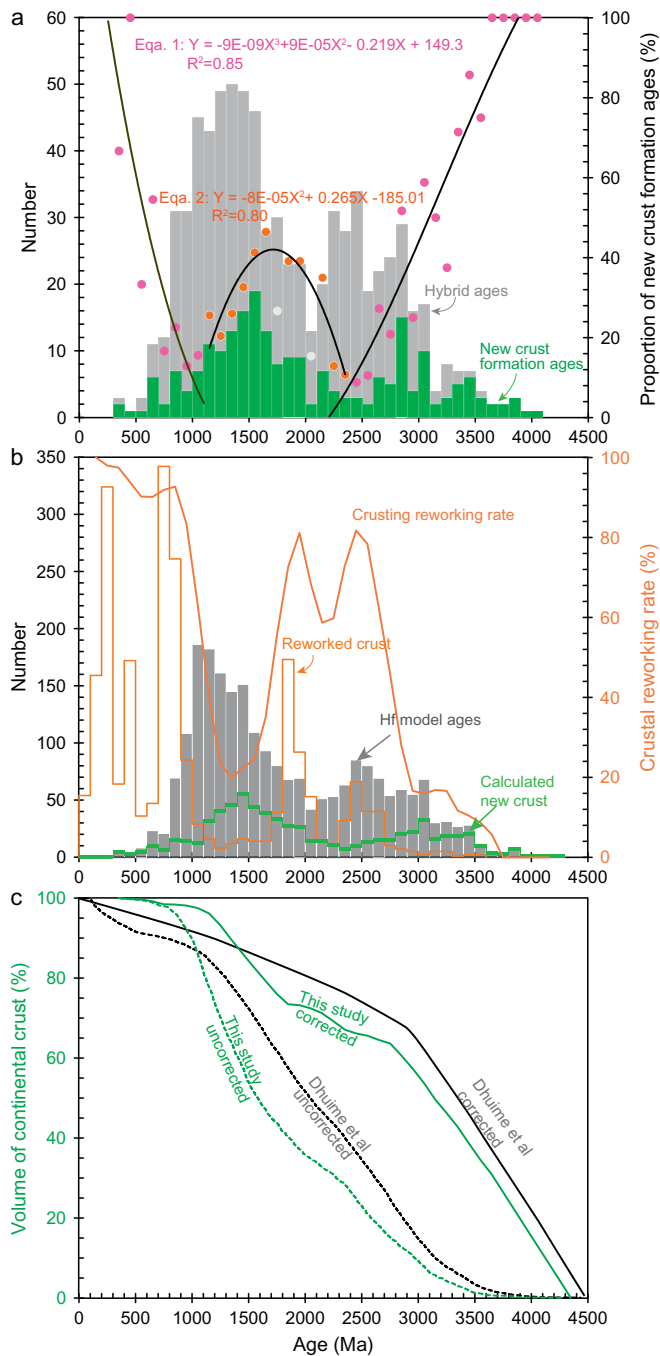
Fig. 12 compares the crustal growth curve for South China with models for the growth of the bulk continental crust. As such it contrasts a crustal growth curve developed from a regional data set with those for global models, and highlights some of the differences. Apart from the curves of Hurley and Rand (1969) and Armstrong and Harmon (1981), the global crustal growth curves are based on studies of detrital zircons. Belousova et al. (2010) utilized detrital zircon U–Pb age and Lu–Hf isotope data to develop two crustal growth curves based on crustal Hf model ages from a global dataset, and on the GLAM (Global Lithospheric Architecture Mapping) model. The crustal growth curves constrained by oxygen isotopes (curve 5 and the green curve) tend to have greater volumes of crust generated by 3 Ga, than those for which O isotopes are not available.

Compared with growth curves based on more global compilations, the curve for South China is more step-like, reflecting periods of increased crustal growth at 1.4–1.6 Ga, and 2.8–3.0 Ga. It therefore has some similarities with the Condie and Aster (2010) curve which is based on the present-day distribution of juvenile rocks of different ages. Significantly, the curve for South China is also similar to the bulk crust growth curve of Dhuime et al. (2012) until the end of the Archaean. This may be because it is more difficult to resolve differences in the growth curves before 3 Ga, or, perhaps because, at least in some models, plate tectonics only became dominant at ~ 3 Ga (e.g. Dhuime et al., 2012; Hawkesworth et al., 2017, 2018), regional variations in crust formation ages only started to develop at that time.
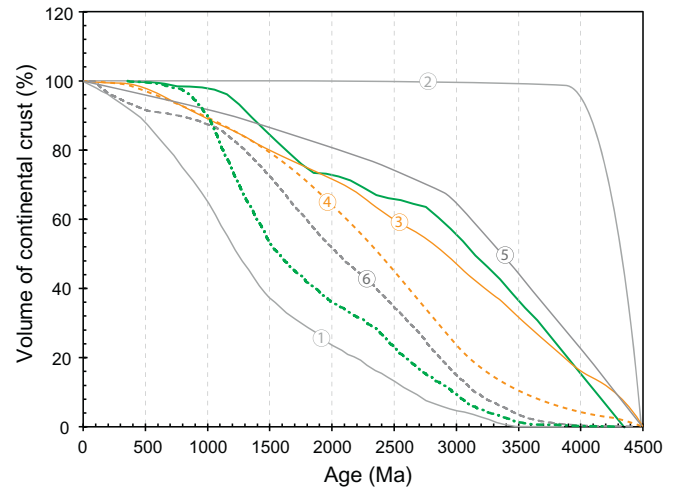
The crustal growth curve for South China (the green solid curve in Fig. 12) shows two inflections, one at ~2.8 Ga and the other at ~1.8 Ga (Fig. 11c, 12). The older inflection at ~2.8 Ga is slightly younger than that of Dhuime et al. (2012) at ~3.0 Ga, which is interpreted to indicate when plate tectonics became dominant. The observed inflection at ca. 3.0 Ga in the crustal growth curve of Dhuime et al. (2012) highlights a change in the rate of crustal growth. There is little evidence for changes in the rates at which new continental crust was generated at that time, and so the reduction in the rate of crustal growth is attributed to an increase in the rates at which continental crust was destroyed. In most models this is linked to plate tectonics becoming the dominant regime controlling crustal growth (e.g. Cawood et al., 2013; Hawkesworth et al., 2017, 2018). Thus the reduction in the rate of crustal growth for South China at ~2.8 Ga may reflect the initiation of plate tectonics in the Yangtze Craton. This would have increased the rates of crustal recycling and hence resulted in the lower crustal growth between ~2.8 Ga and ~1.8 Ga. The younger inflection at ~1.8 Ga marks the onset of another period of increased crustal growth during the Mesoproterozoic at rates similar to those before 2.8 Ga (Figs. 11c, 12). It is taken to be a regional signal in the evolution of South China, which broadly matches with the breakup of the Columbia supercontinent (Zhao et al., 2002). A tectonic switch from collision to extension dominated tectonics also occurred in the Yangtze Craton at ~1.85 Ga (e.g., Peng et al., 2012). This tectonic shift would have led to a decrease in the rates of crust destruction consistent with the onset of another rapid crustal growth period in the Mesoproterzoic. Thus, comparison of the crustal growth curve for South China with growth curves based on more global data sets, highlights the role of tectonics in shaping

Fig. 12. Crustal growth curves of South China (green thick solid and dot-dash curves) taken from Fig. 11, compared with selected curves for the growth of the bulk continental crust. The green thick solid and dot-dash curves are corrected and uncorrected for crustal reworking through time based on oxygen isotopes of detrital zircons. The selected models for continental crustal growth are: 1 Hurley and Rand (1969), 2 Armstrong (1981), 3 and 4 Belousova et al. (2010), 5 and 6 Dhuime et al. (2012). Apart from models 1 and 2, the plotted growth curves are based on studies of detrital zircons. Belousova et al. (2010) compiled the available global detrital zircon U–Pb age and Lu–Hf isotopic data and reported two crustal growth curves based on integration of crustal Hf model ages from a global dataset, and on the GLAM (Global Lithospheric Architecture Mapping) model. However, their results were not constrained by oxygen isotopes and they show gradual growth patterns. Curves 5 and 6 of Dhuime et al. (2012) are corrected and uncorrected for the rate of crust reworking based on $\delta^{18}O$, respectively.

regional growth curves, specifically in the late Archaean and the Mesoproterozoic in South China.

5.5. Variation of oxygen isotopes through time

The oxygen isotopic composition of zircon reflects that of the parent magma. Previous studies have shown that Archean zircons tend to have low $\delta^{18}O$ close to the mantle values (Spencer et al., 2014; Valley et al., 2005), and there is then a marked increase between ca. 2.4 and 2.2 Ga (Spencer et al., 2014; Wang et al., 2009). This has been attributed to increases in the amounts of sediments involved in the source regions of the magmas from which the zircons crystallized (Valley et al., 2005; Wang et al., 2009). Our data reaffirm these general features (Fig. 13), but the maximum $\delta^{18}O$ values appear to follow the estimated variations of atmospheric oxygen levels. These remained persistently low throughout the Archean before the first significant rise between ca.

Fig. 11. (a) Distribution of detrital zircon Hf model ages with mantle-like oxygen isotopes ($\delta^{18}O = 4.7$–6.0‰; Spencer et al., 2014) (green bins) representing new crust formation ages and hybrid model ages with oxygen isotopes outside the mantle-like range (grey bins). The circles represent the proportion of new crust formation ages in time intervals of 100 Ma based on detrital zircons with oxygen isotope data from this study (online supplementary Tables 1 and 2; $n = 448$), volcaniclastic and clastic sedimentary rocks (Wang et al., 2011; $n = 74$), middle to late Permian sediments (Li et al., 2012; $n = 257$) and two Neoproterozoic sedimentary rocks LT07 and GCH01 (X. M. Liu's paper in preparation for submission). The filled pink and orange circles define three curves (black curves), which denote the relationships of the proportion of new crust formation ages through time. Their regressions give Eqa. 1 and Eqa. 2, respectively. Two open circles are not included in the calculation. (b) Distribution of Hf model ages (black histogram), calculated new crust ages (CNCA, green histogram) and reworked crust ages (RCA, orange histogram) based on U–Pb ages and Hf isotope data of detrital zircons from this study ($n = 817$), Yangtze River sands ($n = 808$) (He et al., 2013; Iizuka et al., 2010), volcaniclastic and clastic sedimentary rocks (Wang et al., 2011; $n = 74$), middle to late Permian sediments (Li et al., 2012; $n = 257$), Neoproterozoic sandstones and tillites (Liu et al., 2008; $n = 251$) and two Neoproterozoic sedimentary rocks LT07 and GCH01 (Table 1) in the northern Yangtze Craton (X. M. Liu's paper in preparation for submission). The calculated new crust ages, shown by green bins here, are calculated

by: $N_{CNCA} = N_{Hf\ model\ age} * (Eqa.\ 1)$ and $N_{CNCA} = N_{Hf\ model\ age} * (Eqa.\ 2)$. 'N' in here and below equations represents the number of data for each time interval, and Eqa. 1 and Eqa. 2 are obtained in (a). The reworked crust ages (RCA) are defined as the distribution of zircon crystallization ages that are at least 100 Ma younger than their corresponding Hf model ages, following the equation: $N_{RCA} = N_{(crystallization\ ages\ total)} - N_{(crystallization\ ages=Hf\ model\ ages)}$ (Dhuime et al., 2012). All the ages presented here are calculated in time intervals of 100 Ma. Also shown is the crustal reworking rate (CRR) through time (brown curve), which is calculated from distribution of the proportions of reworked crust (orange histogram) and new crust (green histogram), following the equation: CRR (%) = 100 [$N_{RCA}/(N_{RCA} + N_{CNCA})$]. Thus, the new crust generation rate (NCGR) through time can be obtained by the equation: NCGR (%) = 100-CRR (Dhuime et al., 2012). (c) Crustal growth curves represented by cumulative crust formation ages are calculated using the same dataset as (b). The green dot-dash curve labeled "uncorrected" is cumulative proportions of Hf model ages. The green thick solid curve labeled "corrected" integrates the variations of the reworking rates (brown curve in (b)) in the calculations of the cumulative proportions of the newly formed crust through time. For comparison, also shown are the uncorrected (black dashed curve) and corrected (black thick solid curve) curves of Dhuime et al. (2012) for a worldwide dataset. The model ages in (a, b, c) are calculated for a depleted mantle source.

2.45 and 2.2 Ga, at the Great Oxidation Event (GOE) (Lyons et al., 2014 and references therein). Following Valley et al. (2005), an alternative model is that the step rise in zircon δ^{18}O in the Early Proterozoic, from a limited range in δ^{18}O throughout the Archean, is related to the Great Oxidation Event (GOE). The Archean sediments are dominated by immature volcanoclastic material, which were on average lower in δ^{18}O (Veizer and Mackenzie, 2003), and so there was less elevated δ^{18}O material available to incorporate into the magmas from which the zircons crystallized. Around the Archean/Proterozoic transition, the rise of oxygen and decrease of carbon dioxide in the atmosphere, which may be linked to the emergence of continent during the Neoarchean (Lee et al., 2016), facilitated weathering on the emergent crust and increased the maturity and the clay contents of the clastic sediments, with the result that would have had higher bulk δ^{18}O (Dhuime et al., 2015; Valley et al., 2005; Veizer and Mackenzie, 2003). Incorporation of these more mature sediments in the source of crustally derived magmas would then have resulted in the crystallization of zircon with higher δ^{18}O around the Archean/Proterozoic transition (Fig. 13).

6. Conclusions

Detrital zircons from the upper Yangtze River show concordant age groups at 0–100 Ma, 200–300 Ma, 400–500 Ma, 700–1000 Ma, 1800–1900 Ma and 2300–2500 Ma with a striking peak at 41 Ma diagnostic of magmatism on the Tibetan plateau. Zircons from the middle and lower Yangtze River and its tributaries exhibit broadly similar age groups at 100–300 Ma, 400–500 Ma, 700–900 Ma, 1800–2000 Ma and 2300–2700 Ma, except for the lack of Cenozoic zircons.

The calculated crustal growth curve for South China, following the approach of Dhuime et al. (2012), has two inflections in crustal growth rates at ~2.8 and ~1.8 Ga. The older inflection at ~2.8 Ga is taken to indicate the initiation of plate tectonics in the Yangtze Craton, and it is slightly younger than the estimate of ~3.0 Ga from a global dataset of detrital zircons by Dhuime et al. (2012). The younger inflection at

~1.8 Ga matches the tectonic shift from collision to extension in the Yangtze Craton at ~1.85 Ga. Thus the higher growth rate in the Mesoproterozoic may be related to the breakup of the supercontinent Columbia in the Yangtze Craton. Compared to crustal growth curves based on global data sets (Belousova et al., 2010; Dhuime et al., 2012), the crustal growth curve for South China tends to show more step-like growth patterns, at least since 3 Ga. We propose that crustal growth in South China, at least since ~3 Ga, was controlled by changes in regional geodynamics, leading to changes in the rates of crustal growth, and hence the step-like patterns.

Our zircon oxygen isotopic data show general features of worldwide zircon compilations but with higher δ^{18}O values (Spencer et al., 2014; Valley et al., 2005). The increase in the maximum δ^{18}O values took place at the end of the Archaean when atmospheric O_2 levels were also increasing (Lee et al., 2016; Lyons et al., 2014 and references therein). It is argued that increased weathering resulted in an increase in the volumes of high δ^{18}O sediments which were in turn remobilized in the generation of crustally derived magmas since ~2.5 Ga.

Appendix A. Supplementary data
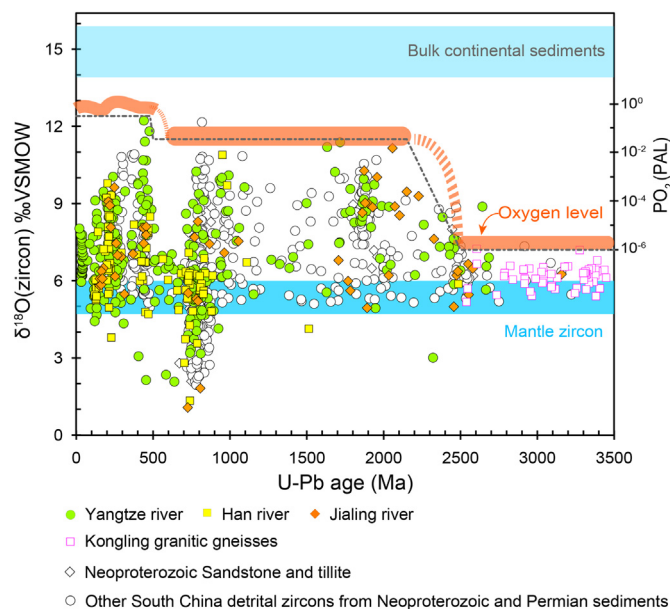
Supplementary data to this article can be found online at https://doi.org/10.1016/j.lithos.2018.09.011.

Fig. 13. Variation of δ^{18}O against crystallization age for detrital zircons from the Yangtze River (filled circles) and its tributaries Han (filled squares) and Jialing (filled diamonds) rivers. Also shown are data for 2.5–3.45 Ga magmatic zircons of granitic gneisses (open squares) from the Kongling Terrane (Guo et al., 2014) and detrital zircons (open circles) from South China (Li et al., 2012; Wang et al., 2011). Dot-dash line is the maximum δ^{18}O envelope of our and Guo et al. (2014) zircons. Horizontal bands show the ranges of mantle-like zircons with δ^{18}O of 4.7–6.0‰ (Spencer et al., 2014) and the bulk continental sediments of δ^{18}O = 14.9 ± 1.0‰ (2σ) (Spencer et al., 2014). The orange band shows the estimated variation of atmospheric oxygen relative to the present atmospheric level (PAL) with the scale on the right (Lyons et al., 2014 and references therein).

References

Amelin, Y., Lee, D.C., Halliday, A.N., Pidgeon, R.T., 1999. Nature of the Earth's earliest crust from hafnium isotopes in single detrital zircons. Nature 399, 252–255.

Amelin, Y., Lee, D.C., Halliday, A.N., 2000. Early-middle archaean crustal evolution deduced from Lu-Hf and U-Pb isotopic studies of single zircon grains. Geochim. Cosmochim. Acta 64, 4205–4225.

Andersen, T., 2002. Correction of common lead in U–Pb analyses that do not report ^{204}Pb. Chem. Geol. 192, 59–79.

Armstrong, R., Harmon, R., 1981. Radiogenic isotopes: the case for crustal recycling on a near-steady-state no-continental-growth earth [and discussion]. Philos. Transac. R. Soc. Lond. 301, 443–472.

Belousova, E.A., Kostitsyn, Y.A., Griffin, W.L., Begg, G.C., O'Reilly, S.Y., Pearson, N.J., 2010. The growth of the continental crust: Constraints from zircon Hf-isotope data. Lithos 119, 457–466.

Black, L.P., Kamo, S.L., Allen, C.M., Davis, D.W., Aleinikoff, J.N., Valley, J.W., Mundil, R., Campbell, I.H., Korsch, R.J., Williams, I.S., 2004. Improved ^{206}Pb/^{238}U microprobe geochronology by the monitoring of a trace-element-related matrix effect; SHRIMP, ID-TIMS, ELA–ICP–MS and oxygen isotope documentation for a series of zircon standards. Chem. Geol. 205, 115–140.

Blichert-Toft, J., Chauvel, C., Albarède, F., 1997. Separation of Hf and Lu for high-precision isotope analysis of rock samples by magnetic sector-multiple collector ICP-MS. Contrib. Mineral. Petrol. 127, 248–260.

Bouvier, A., Vervoort, J.D., Patchett, P.J., 2008. The Lu–Hf and Sm–Nd isotopic composition of CHUR: constraints from unequilibrated chondrites and implications for the bulk composition of terrestrial planets. Earth Planet. Sci. Lett. 273, 48–57.

Bruguier, O., Lancelot, J., Malavieille, J., 1997. U–Pb dating on single detrital zircon grains from the Triassic Songpan–Ganze flysch (Central China): provenance and tectonic correlations. Earth Planet. Sci. Lett. 152, 217–231.

Campbell, I., Hill, R., 1988. A two-stage model for the formation of the granite-greenstone terrains of the Kalgoorlie-Norseman area, Western Australia. Earth Planet. Sci. Lett. 90, 11–25.

Cawood, P.A., Hawkesworth, C., Dhuime, B., 2013. The continental record and the generation of continental crust. Geol. Soc. Am. Bull. 125, 14–32.

Chen, J.F., Jahn, B.M., 1998. Crustal evolution of southeastern China: Nd and Sr isotopic evidence. Tectonophysics 284, 101–133.

Chen, B., Jahn, B.M., Wei, C.J., 2002. Petrogenesis of Mesozoic granitoids in the Dabie UHP complex, Central China: trace element and Nd–Sr isotope evidence. Lithos 60, 67–88.

Chen, S.S., Shi, R., Yi, G.D., Zou, H., 2016. Middle Triassic volcanic rocks in the Northern Qiangtang (Central Tibet): Geochronology, petrogenesis, and tectonic implications. Tectonophysics 666, 90–102.

Claoue-Long, J., Sobolev, N., Shatsky, V., Sobolev, A., 1991. Zircon response to diamond-pressure metamorphism in the Kokchetav massif, USSR. Geology 19, 710–713.

Condie, K.C., Aster, R.C., 2010. Episodic zircon age spectra of orogenic granitoids: The supercontinent connection and continental growth. Precambrian. 180, 227–236.

Dhuime, B., Hawkesworth, C.J., Cawood, P.A., Storey, C.D., 2012. A change in the geodynamics of continental growth 3 billion years ago. Science 335, 1334–1336.

Dhuime, B., Wuestefeld, A., Hawkesworth, C.J., 2015. Emergence of modern continental crust about 3 billion years ago. Nat. Geosci. 8, 552–555.

Dong, Y.P., Zhang, G.W., Neubauer, F., Liu, X.M., Genser, J., Hauzenberger, C., 2011. Tectonic evolution of the Qinling orogen, China: review and synthesis. J. Asian Earth Sci. 41, 213–237.

Elhlou, S., Belousova, E., Griffin, W.L., Pearson, N.J., O'Reilly, S.Y., 2006. Trace element and isotopic composition of GJ-red zircon standard by laser ablation. Geochim. Cosmochim. Acta 70, A158.

Griffin, W.L., Wang, X., Jackson, S.E., Pearson, N.J., O'Reilly, S.Y., Xu, X., Zhou, X., 2002. Zircon chemistry and magma mixing, SE China: in-situ analysis of Hf isotopes, Tonglu and Pingtan igneous complexes. Lithos 61, 237–269.

Guan, Y.L., Yuan, C., Sun, M., Wilde, S., Long, X.P., Huang, X.L., Wang, Q., 2014. I-type granitoids in the eastern Yangtze Block: implications for the Early Paleozoic intracontinental orogeny in South China. Lithos 206, 34–51.

Guo, J.L., Gao, S., Wu, Y.B., Li, M., Chen, K., Hu, Z.C., Liang, Z.W., Liu, Y.S., Zhou, L., Zong, K.Q., 2014. 3.45 Ga Granitic Gneisses From the Yangtze Craton, South China: Implications for Early Archean Crustal Growth. 242. Precambrian Research, pp. 82–95.

Hawkesworth, C.J., Kemp, A.I.S., 2006. Evolution of the continental crust. Nature 443, 811–817.

Hawkesworth, C.J., Dhuime, B., Pietranik, A.B., Cawood, P.A., Kemp, A.I.S., Storey, C.D., 2010. The generation and evolution of the continental crust. J. Geol. Soc. 167, 229–248.

Hawkesworth, C.J., Cawood, P.A., Dhuime, B., Kemp, T.I.S., 2017. Earth's continental lithosphere through time. Annu. Rev. Earth Planet. Sci. 45 (45), 169–198.

Hawkesworth, C., Cawood, P.A., Dhuime, B., 2018. Rates of generation and growth of the continental crust. Geoscience Frontiers (in press and online).

He, S.P., Li, R.S., Wang, C., Zhang, H.F., Ji, W.H., Yu, P.S., Gu, P.Y., Shi, C., 2011. Discovery of 4.0 Ga detrital zircons in the Changdu Block, North Qiangtang, Tibetan Plateau. Chin. Sci. Bull. 56, 647–658.

He, M.Y., Zheng, H.B., Clift, P.D., 2013. Zircon U–Pb geochronology and Hf isotope data from the Yangtze River sands: implications for major magmatic events and crustal evolution in Central China. Chem. Geol. 360, 186–203.

Hu, Z.C., Gao, S., Liu, Y.S., Hu, S.H., Chen, H.H., Yuan, H.L., 2008. Signal enhancement in laser ablation ICP-MS by addition of nitrogen in the central channel gas. J. Anal. At. Spectrom. 23, 1093–1101.

Hu, Z.C., Liu, Y.S., Gao, S., Xiao, S.M., Zhao, L.S., Günther, D., Li, M., Zhang, W., Zong, K.Q., 2012a. A "wire" signal smoothing device for laser ablation inductively coupled plasma mass spectrometry analysis. Spectrochim. Acta B At. Spectrosc. 78, 50–57.

Hu, Z.C., Liu, Y.S., Gao, S., Liu, W.G., Zhang, W., Tong, X.R., Lin, L., Zong, K.Q., Li, M., Chen, H.H., Zhou, L., Yang, L., 2012b. Improved in situ Hf isotope ratio analysis of zircon using newly designed X skimmer cone and jet sample cone in combination with the addition of nitrogen by laser ablation multiple collector ICP-MS. J. Anal. At. Spectrom. 27, 1391–1399.

Hurley, P.M., Rand, J.R., 1969. Pre-Drift Continental Nuclei. Science 164, 1229–1242.

Iizuka, T., Komiya, T., Rino, S., Maruyama, S., Hirata, T., 2010. Detrital zircon evidence for Hf isotopic evolution of granitoid crust and continental growth. Geochim. Cosmochim. Acta 74, 2450–2472.

Jackson, S.E., Pearson, N.J., Griffin, W.L., Belousova, E.A., 2004. The application of laser ablation-inductively coupled plasma-mass spectrometry to in situ U–Pb zircon geochronology. Chem. Geol. 211, 47–69.

Kemp, A.I.S., Hawkesworth, C.J., Paterson, B.A., Kinny, P.D., 2006. Episodic growth of the Gondwana supercontinent from hafnium and oxygen isotopes in zircon. Nature 439, 580–583.

Lee, C.T., Yeung, L.Y., McKenzie, N.R., Yokoyama, Y., Ozaki, K., Lenardic, A., 2016. Two-step Rise of Atmospheric Oxygen Linked to the Growth of Continents (Nature Geosci advance online publication).

Li, X.H., Li, W.X., Li, Z.X., Liu, Y., 2008. 850–790 Ma bimodal volcanic and intrusive rocks in northern Zhejiang, South China: a major episode of continental rift magmatism during the breakup of Rodinia. Lithos 102, 341–357.

Li, X.H., Long, W.G., Li, Q.L., Liu, Y., Zheng, Y.F., Yang, Y.H., Chamberlain, K.R., Wan, D.F., Guo, C.H., Wang, X.C., Tao, H., 2010a. Penglai zircon megacrysts: a potential new working reference material for microbeam determination of Hf-O isotopes and U–Pb age. Geostand. Geoanal. Res. 34, 117–134.

Li, Z.X., Li, X.H., Wartho, J.A., Clark, C., Li, W.X., Zhang, C.L., Bao, C., 2010b. Magmatic and metamorphic events during the early Paleozoic Wuyi-Yunkai orogeny, southeastern

South China: new age constraints and pressure-temperature conditions. Geol. Soc. Am. Bull. 122, 772–793.

Li, X.H., Li, Z.X., He, B., Li, W.X., Li, Q.L., Gao, Y., Wang, X.C., 2012. The Early Permian active continental margin and crustal growth of the Cathaysia Block: In situ U–Pb, Lu–Hf and O isotope analyses of detrital zircons. Chem. Geol. 328, 195–207.

Liu, X.M., Gao, S., Diwu, C.R., Ling, W.L., 2008. Precambrian crustal growth of Yangtze craton as revealed by detrital zircon studies. Am. J. Sci. 308, 421–468.

Liu, Y.S., Gao, S., Hu, Z.C., Gao, C.G., Zong, K.Q., Wang, D.B., 2010. Continental and oceanic crust recycling-induced melt–peridotite interactions in the Trans-North China Orogen: U–Pb dating, Hf isotopes and trace elements in zircons from mantle xenoliths. J. Petrol. 51, 537–571.

Luo, B.J., Zhang, H.F., Lu, X.B., 2012. U-Pb zircon dating, geochemical and Sr–Nd–Hf isotopic compositions of Early Indosinian intrusive rocks in West Qinling, central China: petrogenesis and tectonic implications. Contrib. Mineral. Petrol. 164, 551–569.

Lyons, T.W., Reinhard, C.T., Planavsky, N.J., 2014. The rise of oxygen in Earth's early ocean and atmosphere. Nature 506, 307–315.

Peng, M., Wu, Y., Gao, S., Zhang, H., Wang, J., Liu, X., Gong, H., Zhou, L., Hu, Z., Liu, Y., 2012. Geochemistry, zircon U–Pb age and Hf isotope compositions of Paleoproterozoic aluminous A-type granites from the Kongling terrain, Yangtze Block: Constraints on petrogenesis and geologic implications. Gondwana Res. 22, 140–151.

Peng, T.P., Zhao, G.C., Fan, W.M., Peng, B.X., Mao, Y.S., 2015. Late Triassic granitic magmatism in the Eastern Qiangtang, Eastern Tibetan Plateau: Geochronology, petrogenesis and implications for the tectonic evolution of the Paleo-Tethys. Gondwana Res. 27, 1494–1508.

Pullen, A., Kapp, P., Gehrels, G.E., Ding, L., Zhang, Q., 2011. Metamorphic rocks in central Tibet: lateral variations and implications for crustal structure. Geol. Soc. Am. Bull. 123, 585–600.

Rudnick, R.L., Gao, S., 2003. Composition of the continental crust. In: Heinrich, D.H., Karl, K.T. (Eds.), Treatise on Geochemistry. Pergamon, Oxford, pp. 1–64.

Scherer, E., Münker, C., Mezger, K., 2001. Calibration of the lutetium-hafnium clock. Science 293, 683–687.

Segal, I., Halicz, L., Platzner, I.T., 2003. Accurate isotope ratio measurements of ytterbium by multiple collection inductively coupled plasma mass spectrometry applying erbium and hafnium in an improved double external normalization procedure. J. Anal. At. Spectrom. 18, 1217–1223.

Sláma, J., Košler, J., Condon, D.J., Crowley, J.L., Gerdes, A., Hanchar, J.M., Horstwood, M.S., Morris, G.A., Nasdala, L., Norberg, N., 2008. Plešovice zircon—a new natural reference material for U–Pb and Hf isotopic microanalysis. Chem. Geol. 249, 1–35.

Spencer, C.J., Cawood, P.A., Hawkesworth, C.J., Raub, T.D., Prave, A.R., Roberts, N.M., 2014. Proterozoic onset of crustal reworking and collisional tectonics: Reappraisal of the zircon oxygen isotope record. Geology 42, 451–454.

Sun, W., Li, S., Chen, Y., Li, Y., 2002. Timing of synorogenic granitoids in the South Qinling, Central China: constraints on the evolution of the Qinling-dabie orogenic belt. J. Geol. 110, 457–468.

Valley, J.W., Lackey, J.S., Cavosie, A.J., Clechenko, C.C., Spicuzza, M.J., Basei, M.A.S., Bindeman, I.N., Ferreira, V.P., Sial, A.N., King, E.M., 2005. 4.4 billion years of crustal maturation: oxygen isotope ratios of magmatic zircon. Contrib. Mineral. Petrol. 150, 561–580.

Veizer, J., Mackenzie, F., 2003. Evolution of sedimentary rocks. Treatise on Geochemistry. vol. 7, pp. 369–407.

Vermeesch, P., 2012. On the visualisation of detrital age distributions. Chem. Geol. 312–313, 190–194.

Wang, C.Y., Campbell, I.H., Allen, C.M., Williams, I.S., Eggins, S.M., 2009. Rate of growth of the preserved North American continental crust: Evidence from Hf and O isotopes in Mississippi detrital zircons. Geochim. Cosmochim. Acta 73, 712–728.

Wang, X.C., Li, X.H., Li, Z.X., Li, Q.L., Tang, G.Q., Gao, Y.Y., Zhang, Q.R., Liu, Y., 2011. Episodic Precambrian Crust growth: Evidence From U–Pb ages and Hf–O Isotopes of Zircon in the Nanhua Basin, central South China. Precambrian Research.

Wang, X.X., Wang, T., Zhang, C.L., 2013. Neoproterozoic, Paleozoic, and Mesozoic granitoid magmatism in the Qinling Orogen, China: Constraints on orogenic process. J. Asian Earth Sci. 72, 129–151.

Wang, R.R., Xu, Z.Q., Santosh, M., Liang, F.H., Fu, X.H., 2017. Petrogenesis and tectonic implications of the Early Paleozoic intermediate and mafic intrusions in the South Qinling Belt, Central China: constraints from geochemistry, zircon U–Pb geochronology and Hf isotopes. Tectonophysics 712–713, 270–288.

Weislogel, A.L., Graham, S.A., Chang, E.Z., Wooden, J.L., Gehrels, G.E., Yang, H.S., 2006. Detrital zircon provenance of the Late Triassic Songpan–Ganzi complex: sedimentary record of collision of the North and South China blocks. Geology 34, 97–100.

Wiedenbeck, M., Hanchar, J.M., Peck, W.H., Sylvester, P., Valley, J., Whitehouse, M., Kronz, A., Morishita, Y., Nasdala, L., Fiebig, J., Franchi, I., Girard, J.P., Greenwood, R.C., Hinton, R., Kita, N., Mason, P.R.D., Norman, M., Ogasawara, M., Piccoli, P.M., Rhede, D., Satoh, H., Schulz-Dobrick, B., Skår, Spicuzza M.J., Terada, K., Tindle, A., Togashi, S., Vennemann, T., Xie, Q., Zheng, Y.F., 2004. Further characterisation of the 91500 zircon crystal. Geostand. Geoanal. Res. 28, 9–39.

Woodhead, J., Hergt, J., Shelley, M., Eggins, S., Kemp, R., 2004. Zircon Hf-isotope analysis with an excimer laser, depth profiling, ablation of complex geometries, and concomitant age estimation. Chem. Geol. 209, 121–135.

Xia, L., Li, X.M., Ma, Z.P., Xu, X.Y., Xia, Z.C., 2011. Cenozoic volcanism and tectonic evolution of the Tibetan plateau. Gondwana Res. 19, 850–866.

Xie, G.Q., Mao, J.W., Zhao, H.J., 2011. Zircon U–Pb geochronological and Hf isotopic constraints on petrogenesis of Late Mesozoic intrusions in the southeast Hubei Province, Middle–Lower Yangtze River belt (MLYRB), East China. Lithos 125, 693–710.

Yang, J., Gao, S., Chen, C., Tang, Y.Y., Yuan, H.L., Gong, H.J., Xie, S.W., Wang, J.Q., 2009. Episodic crustal growth of North China as revealed by U–Pb age and Hf isotopes of detrital zircons from modern rivers. Geochim. Cosmochim. Acta 73, 2660–2673.

Yu, J.H., O'Reilly, S.Y., Zhou, M.F., Griffin, W.L., Wang, L.J., 2012. U–Pb geochronology and Hf–Nd isotopic geochemistry of the Badu Complex, Southeastern China: implications for the Precambrian crustal evolution and paleogeography of the Cathaysia Block. Precambrian Res. 222, 424–449.

Zeng, Q.T., McCuaig, T.C., Tohver, E., Bagas, L., Lu, Y.J., 2014. Episodic Triassic magmatism in the western South Qinling Orogen, central China, and its implications. Geol. J. 49, 402–423.

Zhang, H.F., Zhang, L., Harris, N., Jin, L.L., Yuan, H.L., 2006a. U–Pb zircon ages, geochemical and isotopic compositions of granitoids in Songpan-Garze fold belt, eastern Tibetan Plateau: constraints on petrogenesis and tectonic evolution of the basement. Contrib. Mineral. Petrol. 152, 75–88.

Zhang, S.B., Zheng, Y.F., Wu, Y.B., Zhao, Z.F., Gao, S., Wu, F.Y., 2006b. Zircon U-Pb age and Hf-O isotope evidence for Paleoproterozoic metamorphic event in South China. Precambrian Res. 151, 265–288.

Zhang, S.B., Zheng, Y.F., Wu, Y.B., Zhao, Z.F., Gao, S., Wu, F.Y., 2006c. Zircon U–Pb age and Hf isotope evidence for 3.8 Ga crustal remnant and episodic reworking of Archean crust in South China. Earth Planet. Sci. Lett. 252, 56–71.

Zhang, Y.X., Tang, X.C., Zhang, K.J., Zeng, L., Gao, C.L., 2014. U–Pb and Lu–Hf isotope systematics of detrital zircons from the Songpan–Ganzi Triassic flysch, NE Tibetan Plateau: implications for provenance and crustal growth. Int. Geol. Rev. 56, 29–56.

Zhao, G.C., Cawood, P.A., 2012. Precambrian geology of China. Precambrian Res. 222–223, 13–54.

Zhao, J.H., Zhou, M.F., 2008. Neoproterozoic adakitic plutons in the northern margin of the Yangtze Block, China: partial melting of a thickened lower crust and implications for secular crustal evolution. Lithos 104, 231–248.

Zhao, J.H., Zhou, M.F., 2013. Neoproterozoic high-Mg basalts formed by melting of ambient mantle in South China. Precambrian Res. 233, 193–205.

Zhao, G.C., Cawood, P.A., Wilde, S.A., Sun, M., 2002. Review of global 2.1–1.8 Ga orogens: implications for a pre-Rodinia supercontinent. Earth Sci. Rev. 59, 125–162.

Zheng, J.P., Griffin, W.L., O'Reilly, S.Y., Zhang, M., Pearson, N., Pan, Y.M., 2006. Widespread Archean basement beneath the Yangtze craton. Geology 34, 417–420.

Zhou, X.M., Sun, T., Shen, W.Z., Shu, L.S., Niu, Y.L., 2006. Petrogenesis of Mesozoic granitoids and volcanic rocks in South China: a response to tectonic evolution. Episodes 29, 26–32.

Zhou, G., Wu, Y., Gao, S., Yang, J., Zheng, J., Qin, Z., Wang, H., Yang, S., 2015. The 2.65 Ga A-type granite in the northeastern Yangtze craton: Petrogenesis and geological implications. Precambrian Res. 258, 247–259.